Low-Voltage Spatial-Phase-Locked Scanning-Electron-Beam Lithography

by

Lin Lee Cheong

B.Eng., Electrical Engineering (2008), National University of Singapore

Submitted to the Department of Electrical Engineering and Computer Science
in Partial Fulfillment of the Requirements for the Degree of
Master of Science in Electrical Engineering and Computer Science
at the
Massachusetts Institute of Technology
June 2010

ARCHIVES

© 2010 Massachusetts Institute of Technology. All rights reserved

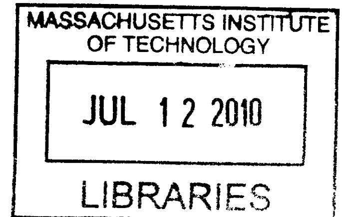

Signature of Author ______________________________

Department of Electrical Engineering and Computer Science
April 29, 2010

Certified by ______________________________

Prof. Henry I. Smith
Professor of Electrical Engineering
Thesis Supervisor

Accepted by ______________________________

Prof. Terry P. Orlando
Chairman, Department Committee on Graduate Students

Low-Voltage Spatial-Phase-Locked Scanning-Electron-Beam Lithography

by

Lin Lee Cheong

Submitted to the Department of Electrical Engineering and Computer Science on April 29, 2010, in partial fulfillment of the requirements for the degree of Master of Science in Electrical Engineering and Computer Science

Abstract

Spatial-phase-locked electron-beam lithography (SPLEBL) is a method that tracks and corrects the position of an electron-beam in real-time by using a reference grid placed above the electron-beam resist. In this thesis, the feasibility of spatial-phase-locked low-voltage electron-beam lithography is investigated. First, the feasibility of low-voltage electron-beam lithography (LVEBL) is experimentally verified using the resists hydrogen silsesquioxane (HSQ) and polymethyl methacrylate (PMMA). Unlike electron-beam lithography at higher voltages, LVEBL has minimal proximity effects and is not resolution-limited by these effects. The fabrication of ultra-thin photoresist grids is investigated and the secondary electron signal levels of these grids are measured.

Thesis Supervisor: Prof. Henry I. Smith

Title: Professor of Electrical Engineering

Acknowledgements

Thanks to my advisor, Prof. Henry I. Smith for taking me under his wing and showing me how *real* research is done. Thanks for your advice on many different matters in life, and for teaching me how to speak coherently, how to trust my instincts, how to think logically and critically, how to write efficiently, how to......

Thanks to Prof. Karl. K. Berggren for always being available and giving good advice when needed.

Thanks to Jim Daley and Mark Mondol for sharing their experiences and knowledge with me, and showing me the ways of Nanostructures Laboratory.

Thanks to my parents and dear brother, who have been incredibly supportive, patient and kept me well-grounded at all times.

Thanks to my officemates, Corey Fucetola and Hasan Korre, for their help, friendship, advice and words of encouragement. I could not have asked for better office-mates. Forge ahead, mates!

Thanks to all the people in Prof. Smith and Prof. Berggren's group. Extra thanks to Vitor Manfrinato, Huigao Duan, Faraz Najafi, Sebastian Strobel, Euclid Moon, Francesco Marsili, Sidney Tsai, Jie Sun, Donny Winston and Tom O'Reilly, for all the laughter and scientific discussions. Additional thanks to Sebastian for helping out with the thesis formatting and layout.

Thanks to all the users in Nanostructures Laboratory.

Thanks to Kizmet, coffee, tea, chocolates, ice-cream and awesome Malaysian food!

Table of Contents

Acknowledgements 5

Chapter 1 Introduction 9

1.1 Scanning-Electron-Beam Lithography (SEBL) 9

1.2 Spatial-Phase-Locked Scanning-Electron-Beam Lithography 13

Chapter 2 Low-Voltage Scanning-Electron-Beam-Lithography 17

2.1 Thin-film Measurements via Ellipsometry 20

2.2 Patterning of Nested L-lines with Low-Voltage Scanning-Electron-Beam Lithography 21

2.2.1 Lithography with Polymethyl Methacrylate (PMMA) 23

2.2.2 Lithography with Hydrogen Silsesquioxane (HSQ) 28

2.3 Monte-Carlo Simulations 33

2.4 Pattern Transfer with HSQ as Etch Mask 39

Chapter 3 SPLEBL Reference Grid Fabrication and Signal Level Measurements 45

3.1 Lloyd's Mirror Interference Lithography 48

3.2 Signal-Level Measurements with sub-2keV Electrons 54

Chapter 4 Conclusion 61

References 63

Chapter 1

Introduction

Lithography is the art of creating desired patterns on a substrate. In the semiconductor industry, the dominant lithographic method is optical-projection lithography (OPL). A radiation-sensitive material, commonly denoted as a *resist*, is first coated on the surface of substrate. The image of a mask, which contains all the desired patterns, is projected onto an ultraviolet (UV)-sensitive resist layer. These patterns are subsequently transferred to the underlying substrate by etching *into* the substrate or depositing material *onto* the substrate, as depicted in Figure 1 [1][2].

Although OPL continues to dominate the integrated-circuit (IC) industry due to its high throughput, the photomasks employed cannot be reliably fabricated solely with diffraction-limited optical methods [3]. Instead, electron-beam lithography (EBL) is used to make these photomasks, and also high-performance devices with ultra-small features [3].

1.1 Scanning-Electron-Beam Lithography (SEBL)

Scanning-electron-beam lithography (SEBL) generates patterns by focusing a beam of electrons onto a resist layer and scanning in a sequential manner. A schematic of a generic SEBL system is depicted in Figure 2. The electron column consists of an emitter that produces a steady stream of electrons that are then accelerated, focused and deflected to the desired location using lenses and deflectors. The electrons are typically accelerated to energies between 10keV and 100keV;

and can be focused into spot sizes <10nm [4]. A beam blanker switches the beam on and off, while deflectors shift the location of the beam as desired. Most of the lenses and deflectors currently employed in SEBL are magnetically controlled, while most blankers are electrostatically controlled [3].

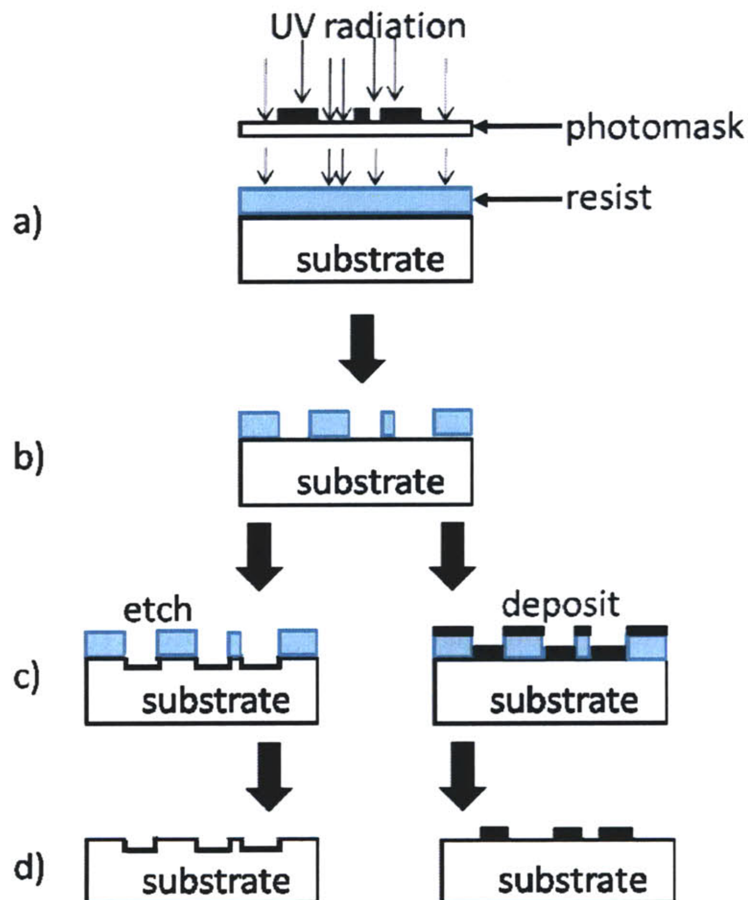

Figure 1. The fabrication process: a) Resist is uniformly spin-coated at high speeds then exposed to UV radiation with a photo-mask. The radiation produces a chemical change in the resist. b) The chemically-altered areas in the resist dissolve at different rates in a developer compared to the unexposed regions, c) subtractive (etching) or additive (deposition) pattern transfer, d) removal of unwanted material such as etch masks and residue photoresist. [2].

Information about the desired pattern is entered into a pattern generator that directs the deflectors and blankers to position the electron beam at the desired locations on the substrate. The substrate itself is placed on a stage with interferometric feedback that allows highly precise (~1nm) stage movements.

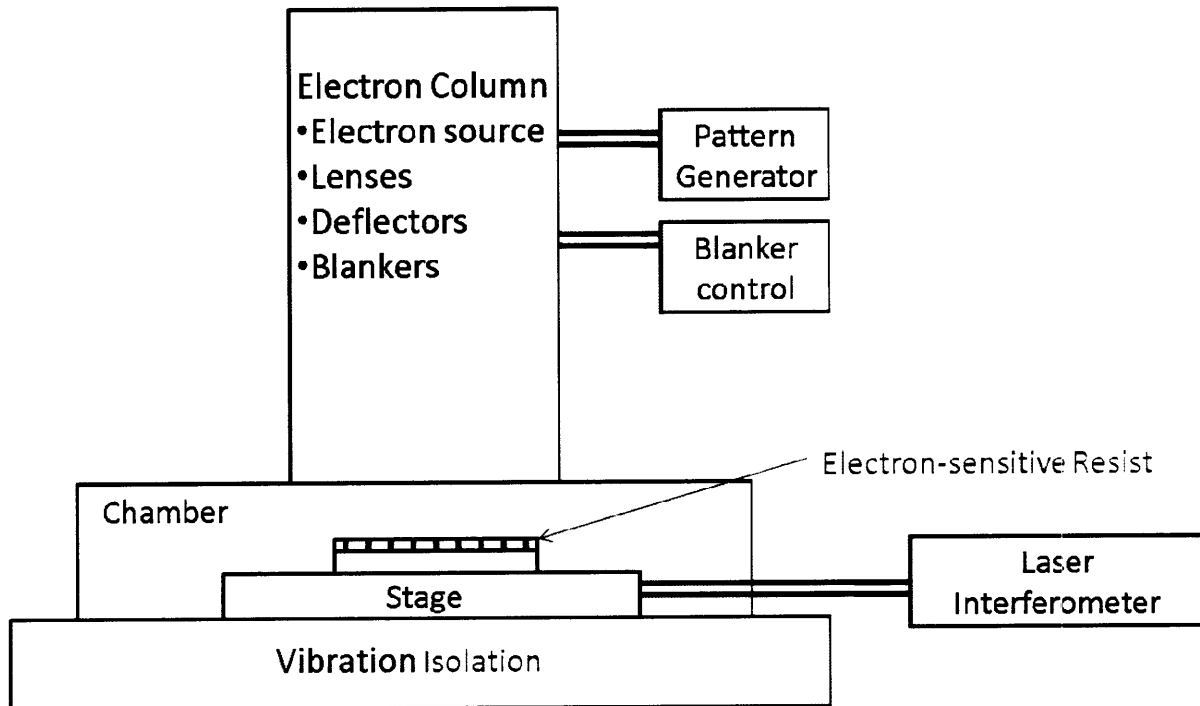

Figure 2. A schematic of a scanning-electron-beam-lithography system. The electron column, combined with the pattern generator and beam blanker, produces a tightly focused beam at desired locations on the electron-sensitive resist on the sample. The sample is placed on a stage controlled with laser interferometers to enable nanometer-precise stage movement. The entire chamber operates under high vacuum and with vibration isolation.

Very small working distances (~ few millimeters) are typically used because spherical-aberrations increase rapidly with distance. Thus, although small electron-beam spot-sizes can be achieved, this is only true over a very limited field. This limited 'write' field poses a serious limitation in electron-beam-lithography, where resolution often must be maintained over

millimeters. Lithographers have partially solved this problem by *stitching*, whereby a pattern larger than a write field is exposed in multiple write fields by translating the highly precise interferometric-controlled stage as necessary.

Thus SEBL, with its sub-nm wavelength and nanometer spot-size, is able to reliably produce patterns with excellent resolution far surpassing the optical diffraction limit. Features as small as 2nm holes at periods of 4nm have been written on metal halides at 100keV [5]. It is also important to note that resists in SEBL systems are exposed directly by the moving beam without the need of any physical masks [4]. The direct-write style of SEBL makes it an excellent research tool as pattern modifications are easily programmed in software.

Although capable of extremely high resolution, all electron-beam systems suffer from a few specific disadvantages compared to OPL. Its slow speed and serial exposure, coupled with the need for high vacuum and high voltage systems, makes SEBL relatively expensive. Another drawback is the *proximity effects* inherent at the voltages commonly used by SEBL. Proximity effects are created by scattering of the electron beam inside the resist and back from the substrate, thereby exposing the resist at unintended locations. In particular, backscattered electrons have relatively wide distribution in space and can cause pattern distortion and loss of resolution around dense features [4][3].

In practice, complex and computationally-intensive programs are used to simulate and correct proximity effects by varying the dose and pattern design. It is interesting to note that proximity effects can actually be reduced at either very high voltages (100keV) or very low voltages around 1keV [6]. At the higher voltages the penetration depth of the electrons is very high, and most of the scattering occurs deep in the substrate, far away from the resist. This reduction in proximity effects comes at a price: the high-energy electrons increase the possibility of substrate damage. Moreover, the effect of backscattered electrons is not eliminated but is just spread out.

At very low voltages (e.g. 1kV), the electrons do not have sufficient energy to generate backscattered electrons. Not only that, the lower electron energy the more of the electron energy is transferred to the resist. This results in a more efficient electron-resist energy transfer and lower chance of substrate damage [7]. Chapter 2 of this thesis investigates the possibility of low-voltage electron-beam-lithography.

1.2 Spatial-Phase-Locked Scanning-Electron-Beam Lithography

Another key problem facing the SEBL community is the poor pattern placement accuracy of EBL systems. Conventional electron-beam tools are fundamentally open-loop systems, and therefore lack the capability to accurately monitor the electron-beam's position relative to the substrate. Laser-interferometer-controlled stages and electro-magnetic deflection systems are insufficient in completely correcting for distortion and drift errors in the system. It is predicted that pattern-placement and field-stitching accuracy will become the limiting factor integrating photonic devices with electronic devices.

Spatial-phase-locked electron-beam lithography (SPLEBL) improves pattern-placement accuracy and field stitching by referencing an electron-transparent periodic grid placed above the resist, as depicted in Figure 3 [8]. The grid provides a real-time feedback signal that enables SPLEBL systems to determine the beam position relative to the substrate. Because secondary-electron detectors are available on some SEBL systems, the secondary-electron signal is preferred as the reference signal. An algorithm determines the actual placement error, and a correction signal is then applied to the deflection system to eliminate positional errors. Pattern-placement as accurate as 1nm has been previously demonstrated via SPLEBL [9].

The requirements for the reference grid itself are fairly stringent: 1) The grid must not interfere with the actual process of resist exposure, 2) The grid must be highly accurate and

precise, 3) The grid must provide a strong enough feedback signal, and 4) the grid must not affect the final resist development process. Currently, the pattern-placement precision of SPLEBL systems is limited by the signal-to-noise ratio (SNR) of the secondary-electron signal from the reference grid. Various materials, such as copper, aluminum, fullerenes and self-assembled monolayers have been investigated in the search for a higher SNR grid [8].

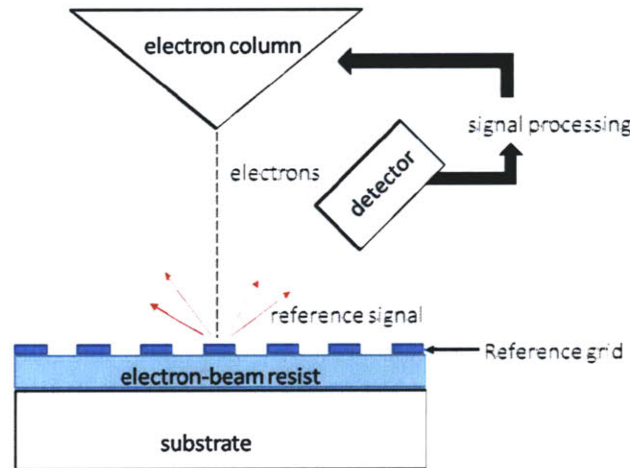

Figure 3. Spatial-Phase-Locked Electron-Beam-Lithography. A reference grid is fabricated on top of the electron-beam resist using interference lithography. Interference lithography is used instead of other lithographic methods due to its accuracy and lack of distortion over long ranges. The radiation that exposes the resist generates a reference signal, usually the secondary electron (SE) signal, when passing through the electron-transparent reference grid to the resist. This signal is recorded by a detector (usually, the SE detector) and then processed to extract information about the electron beam location. The displacement of the actual beam position from the desired position is then calculated and a correction signal is applied to the beam deflection system.

Recently, micro-column-based scanning-electron-beam microscopes have been developed, including the Novelx that was recently purchased by the NanoStructures Laboratory. These systems operate at low voltages (1-2keV), and are fairly low-cost compared to state-of-the-art high-voltage electron-beam lithography systems. Low-voltage systems, combined with spatial-

phase-locking technology, can potentially be transformed into low-cost lithographic tools with good resolution and pattern-placement accuracy. Apart from low-voltage EBL, this thesis also investigates the possibility of using ultra-thin photoresists as a SPLEBL reference grid.

Chapter 2

Low-Voltage Scanning-Electron-Beam Lithography

Limited research has been published in the field of low-voltage electron-beam lithography. Despite that, it is generally accepted that proximity effects are negligible at energies of 2keV and below, and is unlikely to be the limiting factor in achieving high resolution at those energies. Instead, resolution seems to be limited by multiple factors: forward scattering, film type, resist thickness and the intrinsic beam diameter [10][11][12] .

Resist thickness plays a particularly important role in determining resolution due to the small penetration depth of the low-energy electrons. Thin resist modeling suggests that ultra-thin resists are necessary for lithography at 2keV or below [10]. Figure 4 and Figure 5 are Monte Carlo simulations of electron trajectory using 100 electrons entering polymethyl-methacrylate (PMMA) at energies 30keV and 1keV, respectively. Note that the vertical scale in Figure 4 is forty times the scale in Figure 5. All the 100 electrons that entered PMMA at 1keV were stopped less than 30nm from the surface, while the electrons at 30keV were able to penetrate more than 1μm of PMMA easily. Therefore, resists 20nm or thinner are explored in this thesis for low-voltage electron-beam lithography.

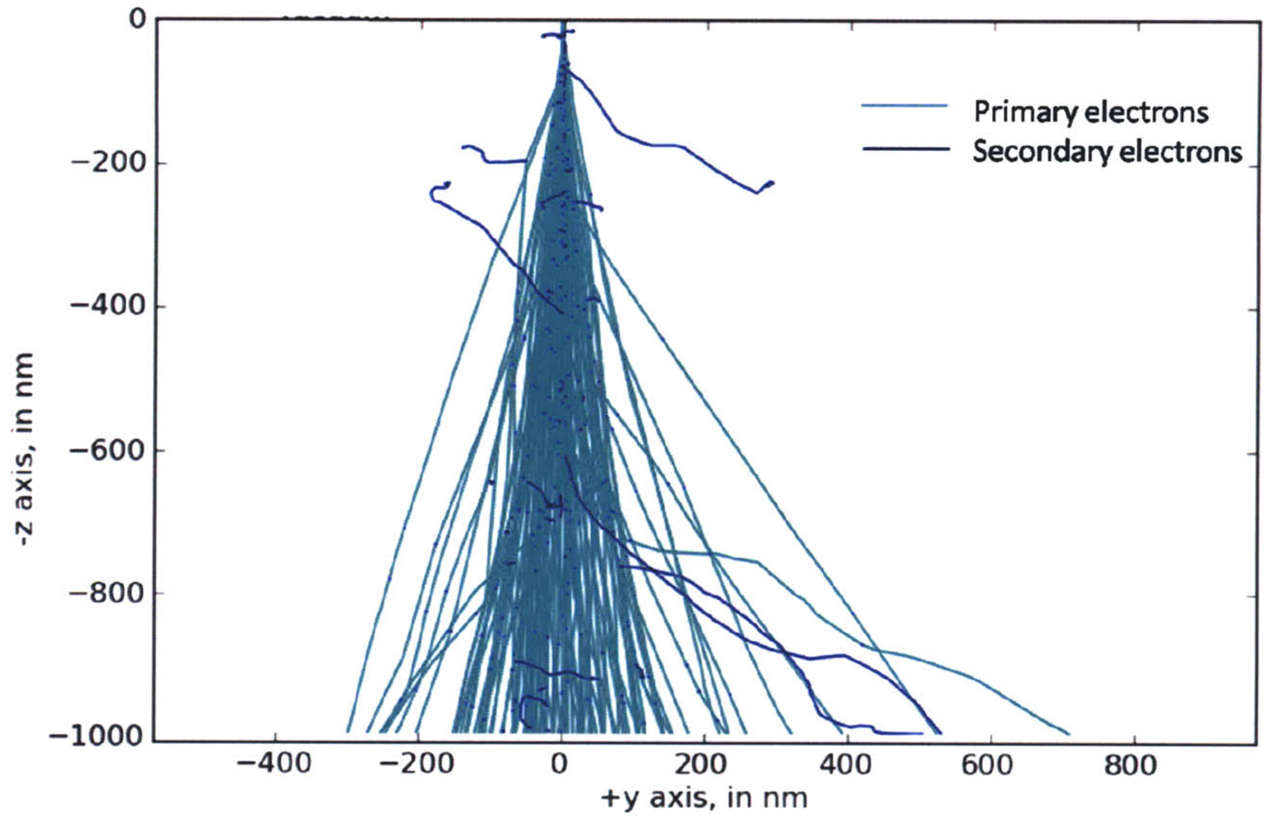

Figure 4 Monte Carlo simulation of electron trajectory with 100 electrons at energy 30keV in PMMA. Forward scattering widens the beam as it traverses through the resist. Note that the vertical scale in this figure is forty times the vertical scale in Figure 5.

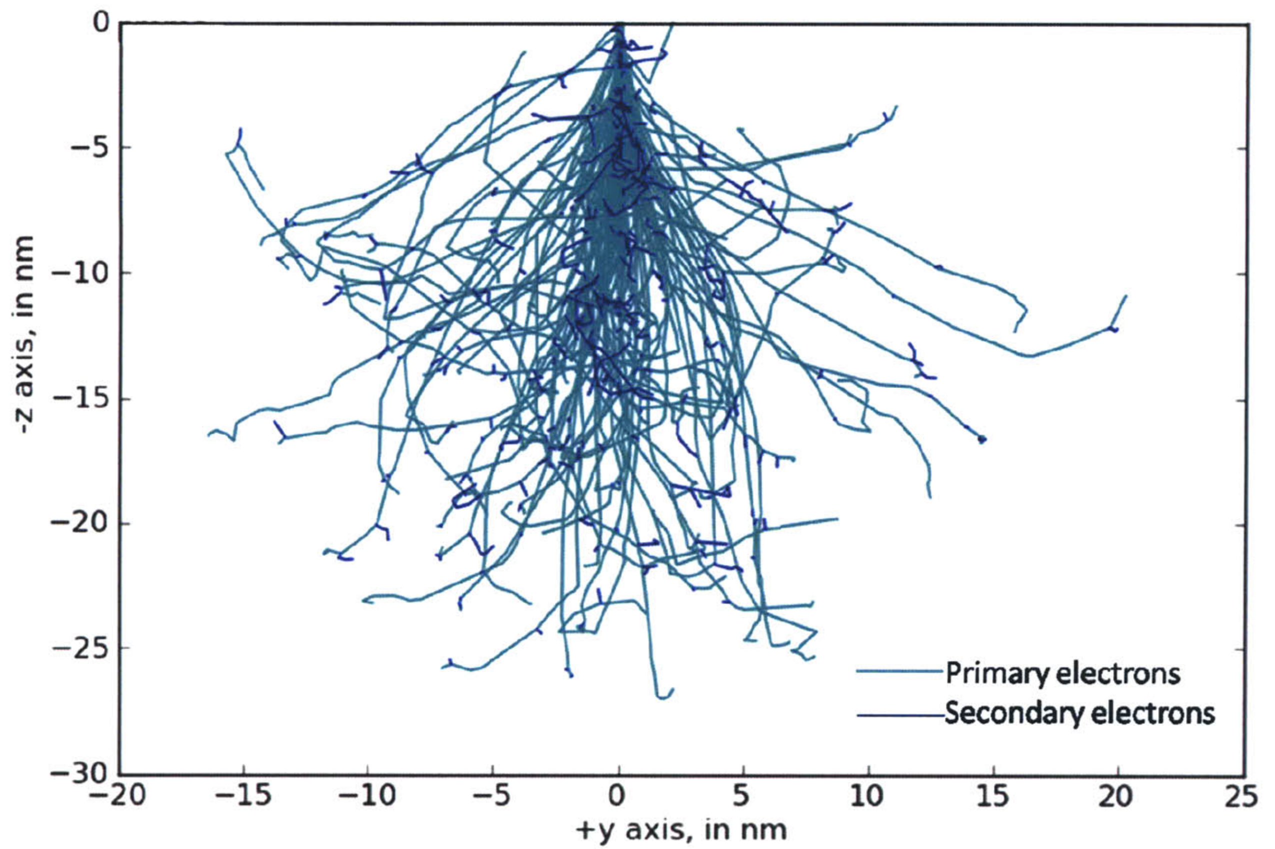

Figure 5 Monte Carlo simulation of electron trajectory with 100 electrons at energy 1keV in PMMA. Note that all the electrons have been stopped in 30nm of resist while the electrons in Figure 4 have successfully traversed at least 100nm of resist.

2.1 Thin-film Measurements via Ellipsometry

Ellipsometry has been used widely to characterize thin films. It is capable of measuring nanometer-thick uniform films on a bulk substrate [13][14]. Spectroscopic ellipsometry, which characterizes films using multiple wavelengths, is capable of collecting a range of useful data about a sample [14]. These data can then be used to fit known material models and measure film thicknesses with enhanced accuracy.

Ellipsometers operate by detecting the change in the phase of a polarized beam of light reflected from a sample surface [14]. Two values related to the Fresnel reflection coefficients are measured; psi (Ψ) and delta (Δ). They are related by $\rho = \frac{R_p}{R_s} = \tan(\Psi)e^{i\Delta}$, where R_p and R_s are the reflection coefficients for *p*- and *s*-polarized light.

After the Ψ and Δ are measured, a model based on the Kramers-Kronig relations is then constructed using the known parameters, including incident wavelength, angle of incidence and polarization state. The ellipsometer software then simulates the model and obtains a best-fit value for the film-thickness. Sometimes, tabulated optical constants of known materials may be used. Because diluted materials were extensively used in this investigation, function-based models (Cauchy model and general oscillator model) were used to model the film thickness and optical constants of the thin films. All ellipsometric measurements in this thesis of film thicknesses and optical constants were obtained using the J. A. Woollam spectroscopic ellipsometer at the Institute of Soldier Nanotechnologies (ISN) at MIT. Figure 6 is a plot of experimental and simulated psi and delta values of a hydrogen silsesquioxane (HSQ) layer.

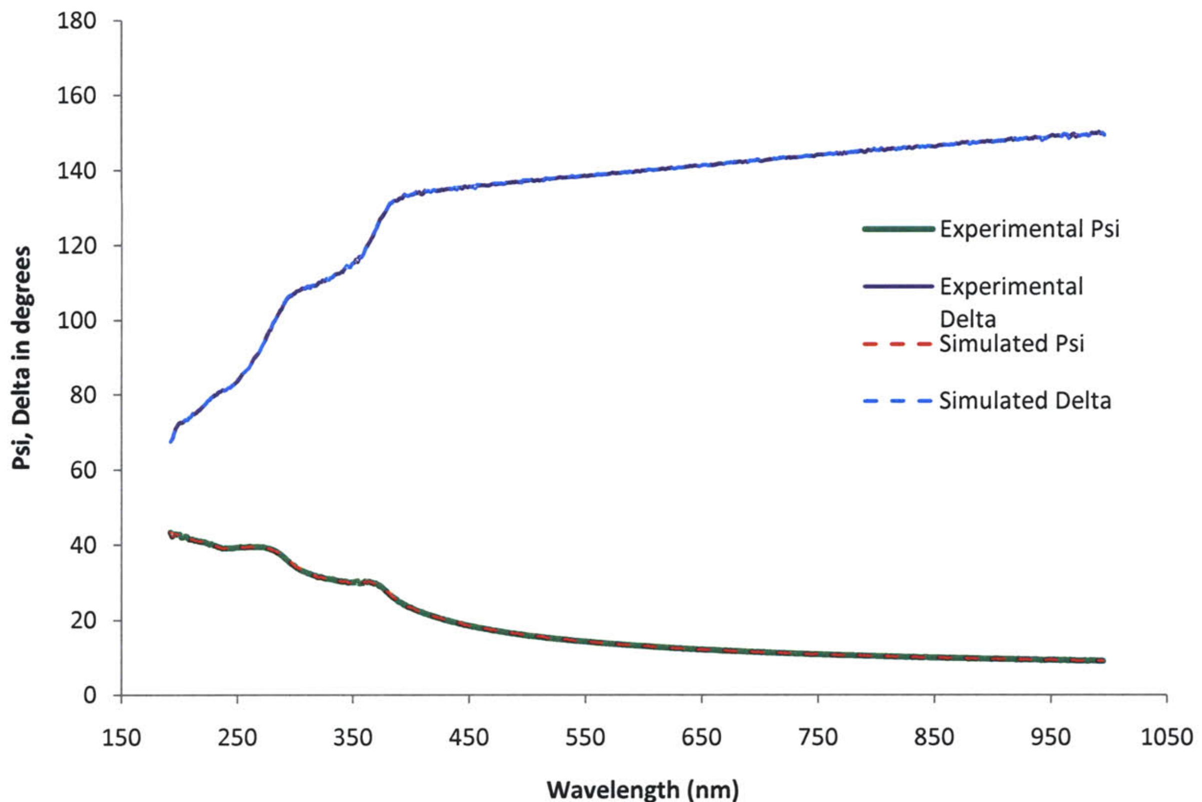

Figure 6. Simulated and experimental psi and delta. Dotted lines indicate the fitted psi and delta values using a Cauchy model. The film thickness parameter was determined by finding the minimum of the mean squared error (MSE) between the modeled and experimental values. In this figure, the experimentally-determined psi and delta overlap with the modeled values, indicating a good fit and hence a good estimation of the film thickness.

2.2 Patterning of Nested L-lines with Low-Voltage Scanning-Electron-Beam Lithography

Many different materials have been explored as electron-beam resists over the past decades. Commonly used electron-beam resists for scanning-electron-beam lithography (SEBL) include organic resists such as polymethyl methacrylate (PMMA), calixarene and poly (α-chloro-acylate-

co-α-methyl styrene), also commercially known as ZEP520; and inorganic resists such as hydrogen silsesquioxane (HSQ) [1][15]. Metal halides and metal oxides have also been used as SEBL resists, with 2nm diameter holes at 4nm pitch fabricated on 80nm thick AlF_s film at energy of 100keV. Although metal halides and oxides have the highest resolution reported to date, they suffer from problems like reproducibility and pattern instability. Hence, metal halides and oxides will not be explored further in this thesis. All the electron-beam lithography reported in this thesis was done with the Raith 150 at the Scanning-Electron-Beam Lithography Facility (SEBL).

Materials such as HSQ, PMMA, calixarene and ZEP-520 have been used as resists for low-voltage scanning-electron-beam lithography [10][11][12][1]. In terms of pushing the resolution limits at low voltages, *Jamieson et. al.* patterned 30nm lines at 60nm periods using 24nm-thick HSQ at 2keV [16]. Lines, 40nm wide, have been also patterned in PMMA, while 10nm wide lines have been patterned with calixarene at 2keV [10][11].

Nested L's are used in this thesis instead of single lines to investigate the resolution of scanning-electron-beam lithography because proximity effects become evident with dense patterns. L-shaped lines, shown in Figure 7, are used to indicate lithographic capabilities in orthogonal directions.

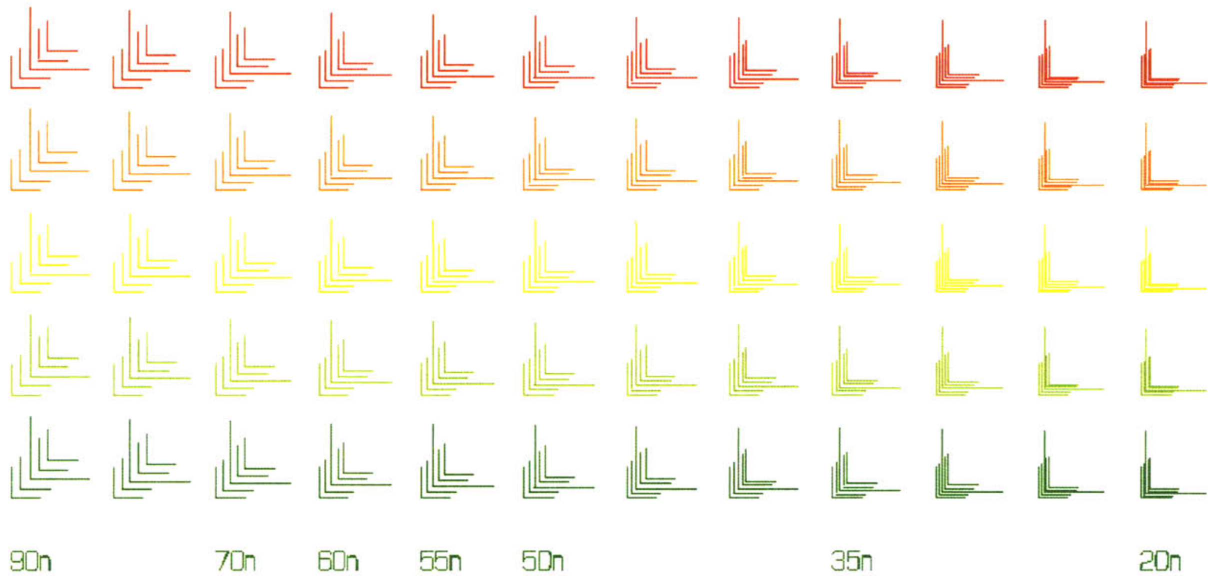

Figure 7. A pattern file of nested L-lines used in some of the resolution tests in this thesis. The period between the lines is decreasing from left to right, while the changing color from green to red indicates an increasing dose.

2.2.1 Lithography with Polymethyl Methacrylate (PMMA)

PMMA, a commonly used polymer in everyday life, is a positive-tone electron-beam resist that has been used reliably for decades [17]. When exposed to electron radiation, its long polymeric chains undergo scissation. These fragmented sections of the polymer dissolve more readily than the unexposed polymer chains in certain solvents, usually methyl isobutyl ketone (MIBK). Under extremely high electron dose, the fragmented sections of the exposed polymer cross-link and PMMA becomes a negative-tone resist.

PMMA of molecular weight 950,000 was used in the following experiments. The polymer was first dissolved in anisole to 0.5 wt %, and then spin-coated at 5krpm on a silicon wafer to a thickness of roughly 11nm. Prior to spin-coating, the wafer was exposed to UV-ozone for 10 minutes. This step is performed because steam nucleation tests indicate the presence of organic

residue on new silicon wafers used in these experiments. Because adhesion of very thin films to silicon wafers is sensitive to the surface cleanliness, it is important to ensure that the silicon wafers are contaminant-free prior to spin-coating. Exposure to UV-Ozone removes the organic contaminants from the silicon surface.

After spin-casting, the wafer was then baked at 180°C for 90s to remove the anisole solvent. After patterning via SEBL, the sample was then developed in MIBK and isopropanol (IPA) solution at 21°C for 30s. The ratio of MIBK to IPA was 1:3. Development was stopped by spraying IPA onto the sample, followed by blow drying with nitrogen. A thin conducting gold layer was then sputtered onto the developed structures to facilitate the SEM imaging process.

Nested L-lines were patterned into PMMA at energies 2keV, 1.5keV and 1keV. An initial dose-matrix test indicated that the dose required for exposure at the mentioned voltages was very low, indicating a very efficient energy transfer between the electron beam and PMMA. An electron dose of 45pA/cm was applied for all exposures. Sets of seven nested L-lines were patterned at 2keV electron energy with varying pitch. As seen in Figure 8, the lines were well defined and easily patterned at 100nm pitch.

Figure 8. Nested L-lines at 100nm pitch in 11nm thick PMMA on silicon using an electron beam of energy 2keV. Resist was developed in MIBK: IPA ratio of 1:3 for 30s, and the developed L-lines are well-defined. Samples were sputter-coated with gold-palladium to improve image contrast.

At pitches between 25nm and 90nm, sets of five shorter nested L-lines were also patterned at 2keV. Lines at pitches 90nm, 80nm and 70nm were successfully resolved, as shown in Figure 9. The white specks observed in Figure 9 are redeposited contaminants from colloidal gold that

was used for focusing during the electron-beam exposure. It was not possible to resolve lines at 60nm or below. Although lowering the delivered dose may possibly result in denser patterns, this was not possible as 45pA/cm is the smallest dose the Raith 150 SEBL system is capable of delivering to any resist at low voltages.

Similar results were obtained from exposures at electron energies of 1.5keV and 1keV. At both energies, nested L's at 70nm pitch were resolvable but not at 60nm pitch. Figure 10 and Figure 11 show micrographs of nested lines at varying pitches at energies of 1.5keV and 1keV, respectively.

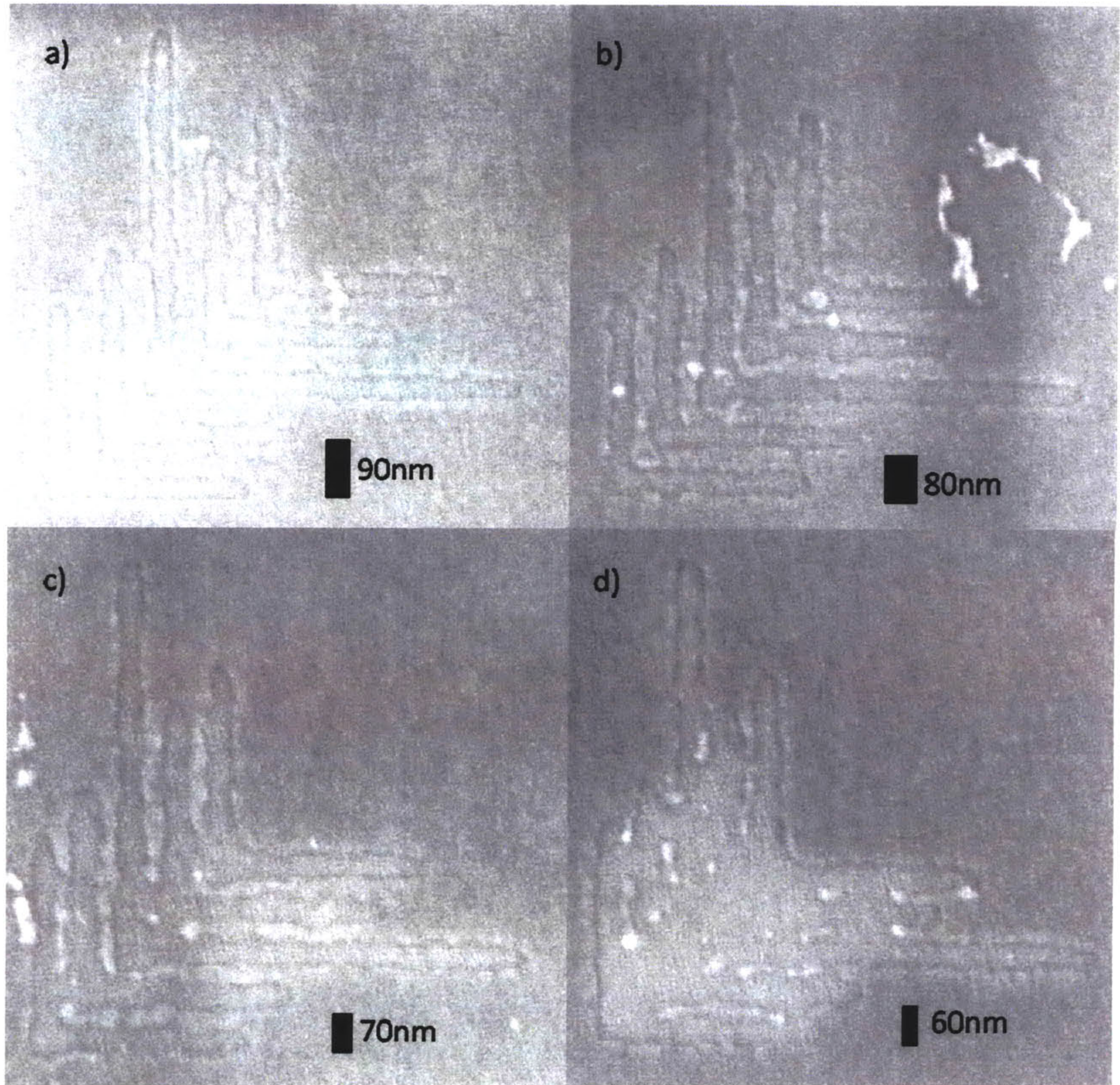

Figure 9. Nested L-lines at pitches of a) 90nm, b) 80nm, c) 70nm and d) 60nm patterned at energy 2keV on 11nm-thick PMMA on silicon. Resist was developed in MIBK:IPA ratio of 1:3 for 30s and then gold-palladium sputtered for image contrast. L-lines as close as 70nm could be resolved.

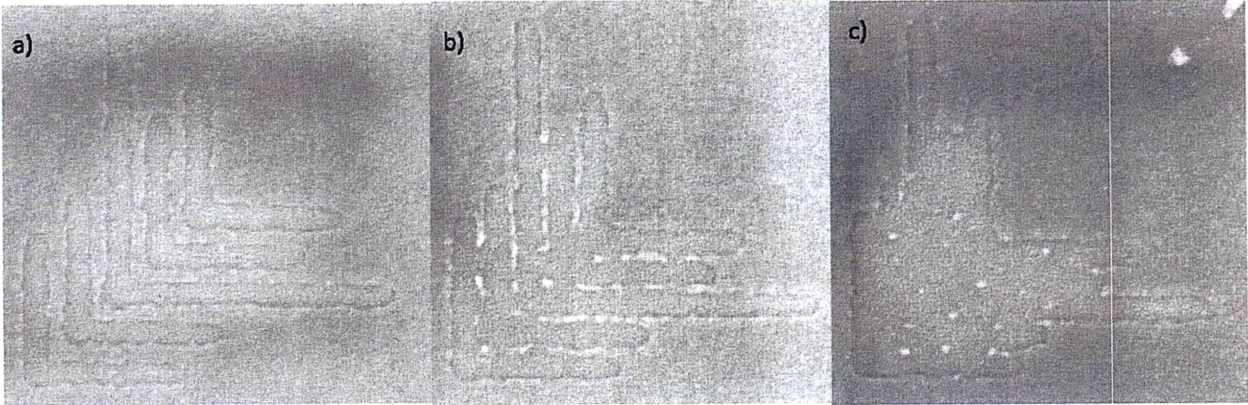

Figure 10. Nested L's patterned in 11nm-thick PMMA on silicon at electron energy 1.5keV with pitches of a) 90nm, b) 70nm and c) 60nm. L-lines with periods of 90nm and 70nm were resolvable. Variations in the background of the images originate from carbon deposition on the sample during imaging.

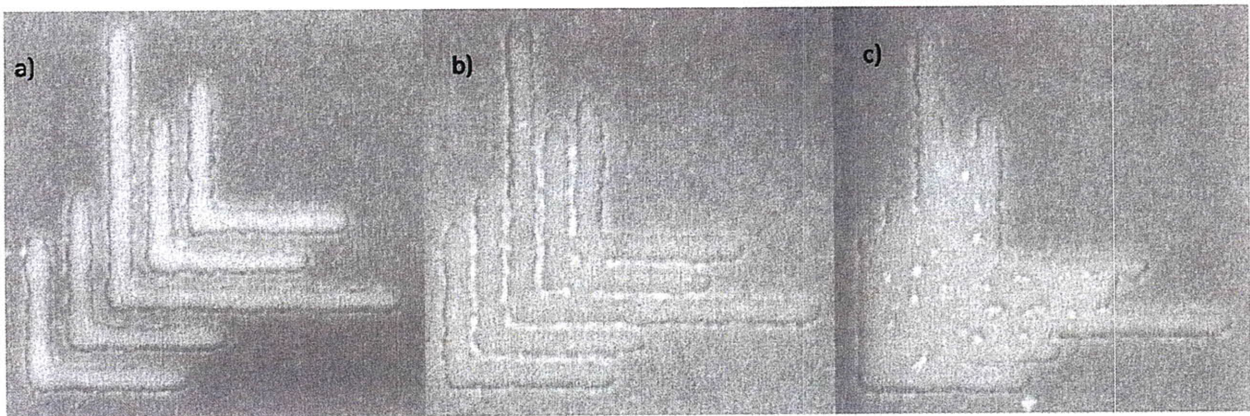

Figure 11. Nested L's patterned in 11nm-thick PMMA on silicon at 1keV electron energy with pitches of a) 90nm, b) 70nm and c) 60nm. L-lines with periods of 90nm and 70nm were resolvable.

2.2.3 Lithography with Hydrogen Silsesquioxane (HSQ)

Hydrogen silsesquioxane (HSQ) is a negative-tone electron resist that was first investigated in 1998 [18]. HSQ contains elements silicon, oxygen and hydrogen in a network of partially formed

cages. A schematic of the cage-like structure is shown in Figure 12 [1]. After electron-beam exposure, HSQ undergoes chemical changes and reorganizes as silicon dioxide.

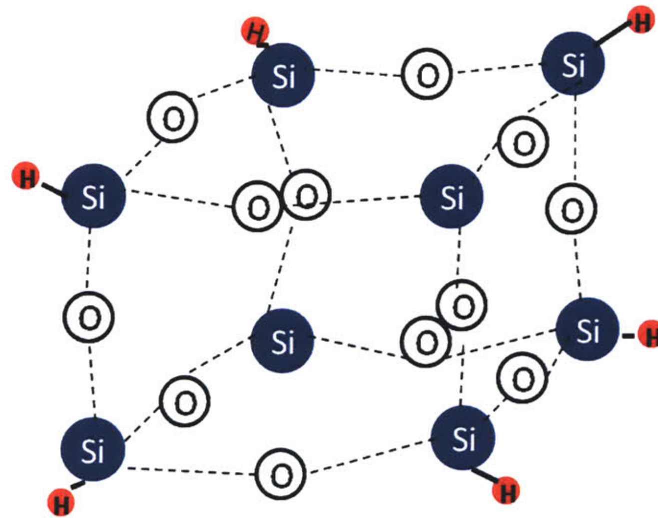

Figure 12. Cage structure of HSQ, a spin-on glass manufactured by Dow Corning. HSQ forms a network of partially-formed cages when spin-coated onto a substrate.

Of all the resist materials, HSQ seem to hold the most promise as a high-resolution, low-voltage, electron resist, due to its high contrast, low sensitivity relative to PMMA and thin film uniformity [1]. HSQ, 24nm thick, was patterned to 30nm lines at 60nm period at 1keV by Jamieson *et. al.* [16]. This result is currently the best resolution reported for dense features at 2keV or below [16].

The HSQ (1% diluted in MIBK) used in the following experiments was obtained from Dow Corning Corporation. A silicon wafer was first subjected to UV-ozone treatment for 10 minutes to remove organic contaminants from the surface. After the surface was certified clean by a steam nucleation test, HSQ was spin coated onto the surface at 5000 rpm. The HSQ layer was found to be 14.6nm thick via ellipsometry. Nested L's were then patterned into the resist via SEBL and subsequently developed using salty developer, consisting of 4% sodium chloride and 1%

sodium hydroxide in de-ionized (DI) water [19]. Unexposed regions are highly soluble in the sodium-chloride/sodium-hydroxide mixture, while the radiation-exposed regions (silicon dioxide) are insoluble. Samples were immersed in the salty developer for one minute, rinsed with DI water, and then blown dry with nitrogen.

Nested L's were patterned in HSQ on silicon at energies 2keV, 1.5keV and 1keV; the same energies that were used to pattern PMMA, as reported in the previous section. The clearing dose required for HSQ is an order of magnitude higher than that of PMMA, but a higher resolution was achieved for dense features. Dose matrices of nested L's, from 400pA/cm to 900pA/cm were written at 2kV voltage, as shown in Figure 13, using the test pattern shown in Figure 7. The lines have reducing periods from left to right, with the leftmost nested L-lines having a pitch of 90nm and the rightmost with a pitch of 20nm.

Dense lines with pitches that were challenging to resolve in PMMA could be easily resolved when written in HSQ. Figure 14 shows micrographs of the nested L's that were written at 600pA/cm with periods of 30nm, 25nm and 20nm respectively. Thus, dense features with 20nm periods can be written at 2kV voltage. Nested L-lines of 20nm period were also successfully written at 1.5kV while the smallest period possible at 1kV was 25nm. Figure 15 and Figure 16 are micrographs of the nested L-lines exposed at 1.5kV and 1kV, respectively.

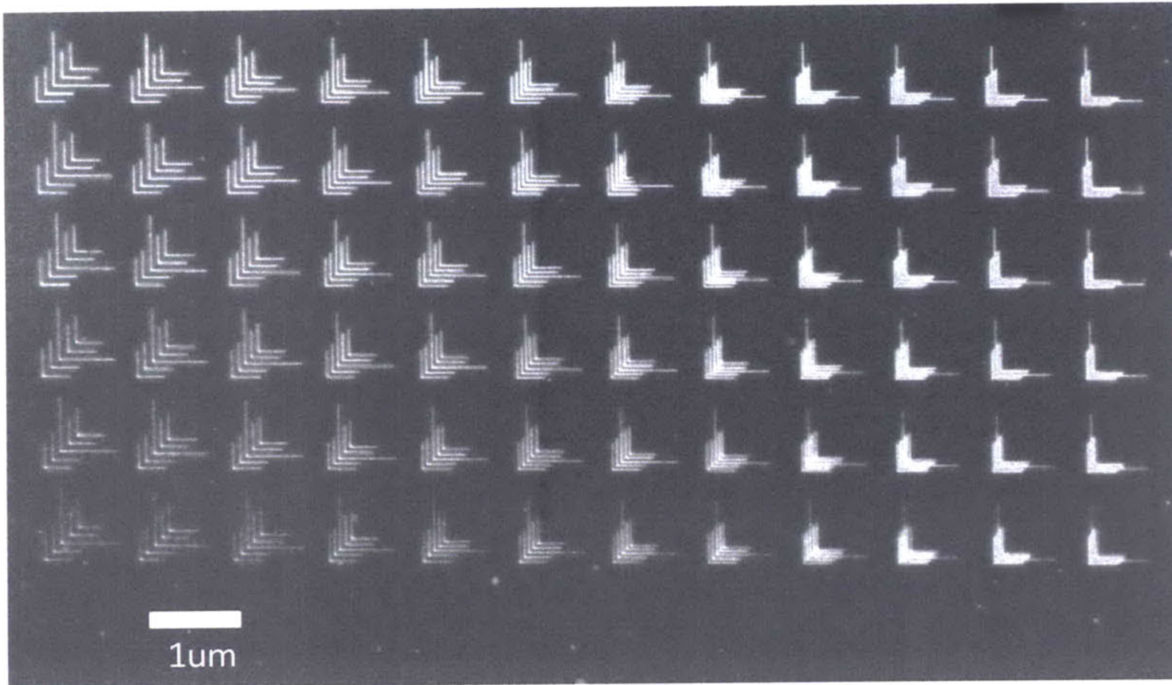

Figure 13. Dose matrix of nested L-lines from 600pA/cm (lowest row) to 900pA/cm (highest row) in steps of 60pA/cm.

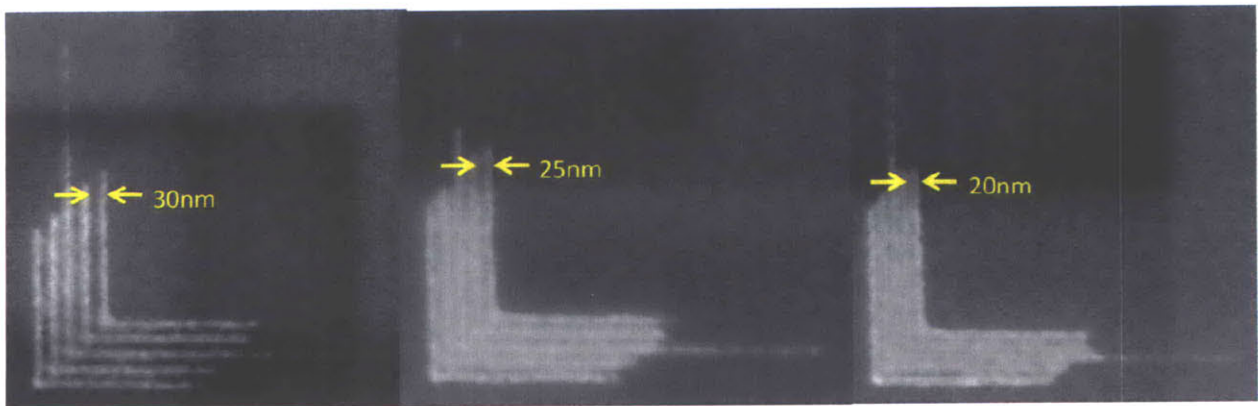

Figure 14. Nested L-lines of pitch 30nm, 25nm and 20nm written with energy 2keV in almost 15nm thick HSQ on silicon, developed using salty developer for one minute.

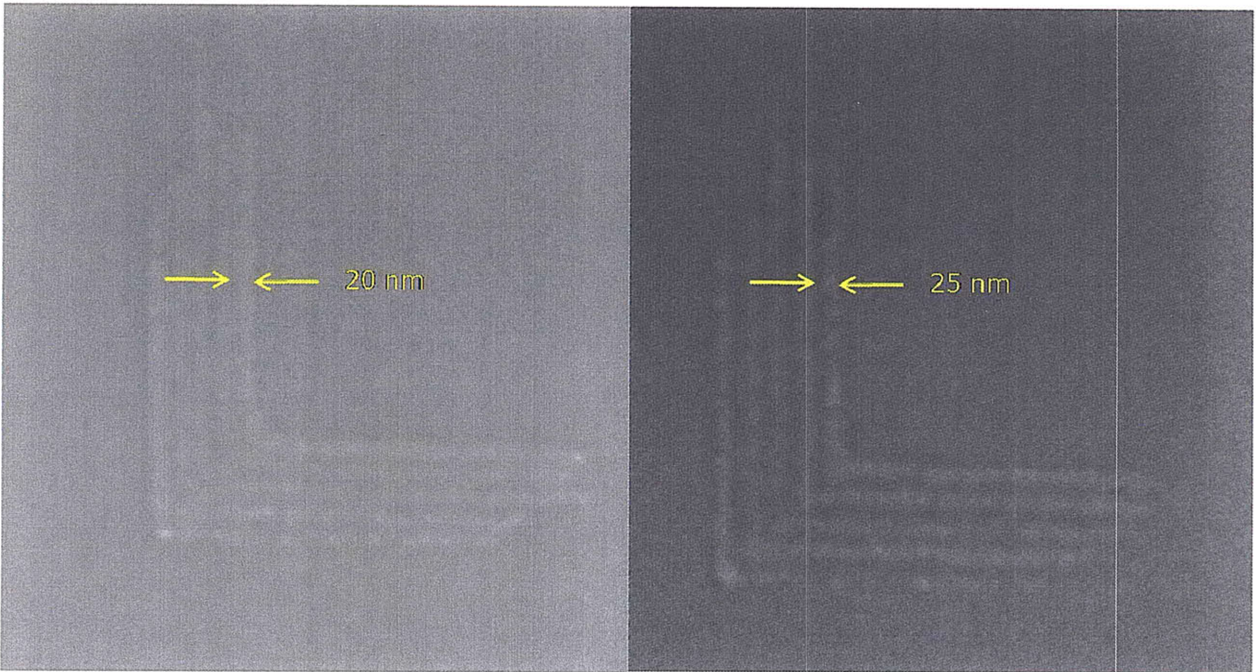

Figure 15. Nested L's with 20nm and 25nm pitch exposed at 1.5kV in ~15nm of HSQ on silicon (developed with salty developer). The smallest pitch attainable at this voltage is 20nm.

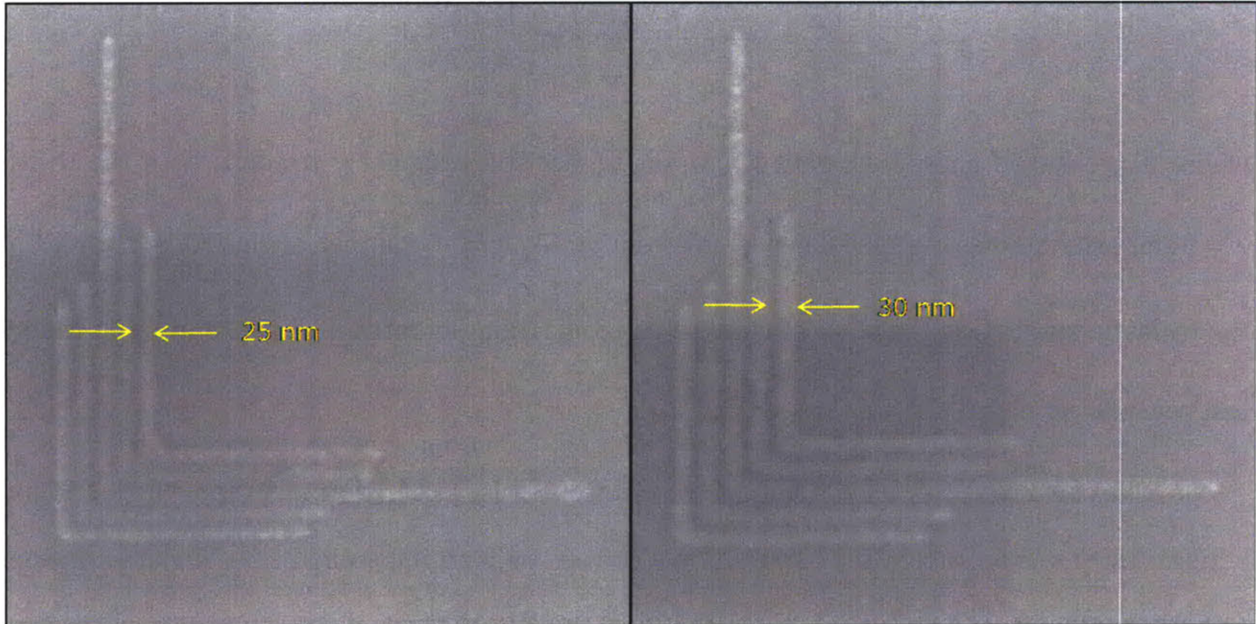

Figure 16 Nested L's with 25nm and 30nm pitch exposed at 1kV in ~15nm of HSQ on silicon (developed with salty developer). The smallest pitch attainable at this voltage is 25nm, slightly worse resolution compared to the 20nm pitch achieved using a beam energy of 2keV and 1.5keV.

2.3 Monte-Carlo Simulations

This section focuses on simulations of interactions between the exposing electron beam and the resist at voltages of 1kV, 1.5kV and 2kV. Point-spread functions plot the spatial distribution of the energy deposited into a material by a beam of electrons exposing a stationary spot. In contrast, line-spread functions plots the cross-sectional spatial distribution of energy deposited when a beam of electrons exposes a resist with a continuous line-scan. Point-spread functions, line-spread functions and the dose distribution of multiple lines were simulated to model the energy transfer from the electron to the resist. The simulation codes in C used were written by Ray Ghanbari and subsequently modified by Juan Ferrera [20].

The interaction between an electron beam and the resist at low energies is described by the modified Bethe's equation

$$\frac{dE}{dl} = -\frac{2\pi e^4 n N_{eff}(E)}{E} \ln\left(\frac{1.166E}{I_{eff}(E)}\right)$$

where $E =$ electron energy, $l =$ path length along electron trajectory, $\rho =$ density of the resist, $n =$ number of atoms or molecules per unit volume, $N_{eff}(E) =$ number of electrons involved in the inelastic interaction, $I_{eff}(E) =$ effective mean ionization potential of resist or average energy lost per interaction [21].

The substrate layer used to model the electron-resist interaction was 14nm-thick HSQ on a 20μm-thick silicon substrate. Two million electrons with an incoming beam diameter of 8nm (similar to the actual beam diameter in the Raith 150) were tracked as they traversed through the sample. Secondary electrons generated by the incident beam were also considered in the model. The electrons were considered to have been stopped by the sample when the incident energy fell to 50eV.

Point-spread functions (PSF) at the HSQ-silicon interface for incident energies of 1keV, 1.5keV and 2keV are shown in Figure 17. The full-width half-maximum (FWHM) of the PSF widens with decreasing incident energy. At distances far away from the beam entry location the amount of energy deposited is inverted: higher (2keV) incident-energy electrons deposit more of their energy compared to lower (1keV) incident-energy electrons. This is consistent with the fact that proximity effects become more evident as the incident electron energy increases. Line-spread functions, depicted in Figure 18, also show a similar trend.

Line-spread function of an incoming 2keV electron beam was used as the basis to model the energy distribution of five lines written on 14nm-thick HSQ on silicon, conditions that were used experimentally in the previous section of this thesis. This line-spread function was convolved with five discrete impulses at intervals of 20nm to produce the energy profile shown in Figure 19. The red horizontal line indicates the amount of energy necessary for the HSQ resist to convert to

silicon dioxide. This value was determined by comparing single-pass lines experimentally written in HSQ at 2keV with the line-spread function generated under similar conditions. The width of the lines was experimentally determined to be approximately 9nm, which was then used to establish the minimum amount of energy necessary to crosslink HSQ. In this figure, the amount needed for crosslinking is slightly higher than the energy deposited in between the lines, and is consistent with experimental results (minimum resolvable pitch of 20nm).

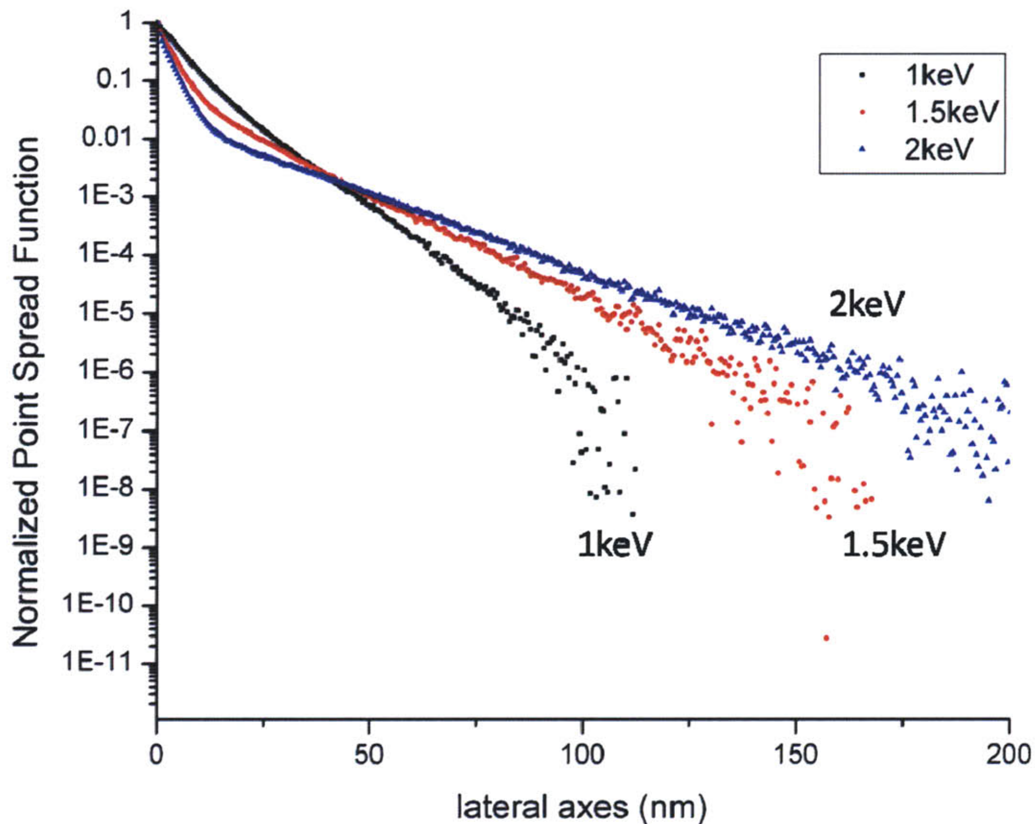

Figure 17. Normalized point spread function with incident energies of 1keV, 1.5keV and 2keV. The electrons were incident on a 14nm thick HSQ layer on silicon, with an input beam diameter of 8nm. Two million incoming electrons, including the generated secondary electrons were tracked as it passed through the sample. The 2kV PSF has the smallest full width half maximum, and the 1kV PSF has the widest. This is consistent with experimental results, with the smallest pitch of dense lines patternable at 2kV being 20nm and the smallest pitch possible at 1kV increasing to 25nm.

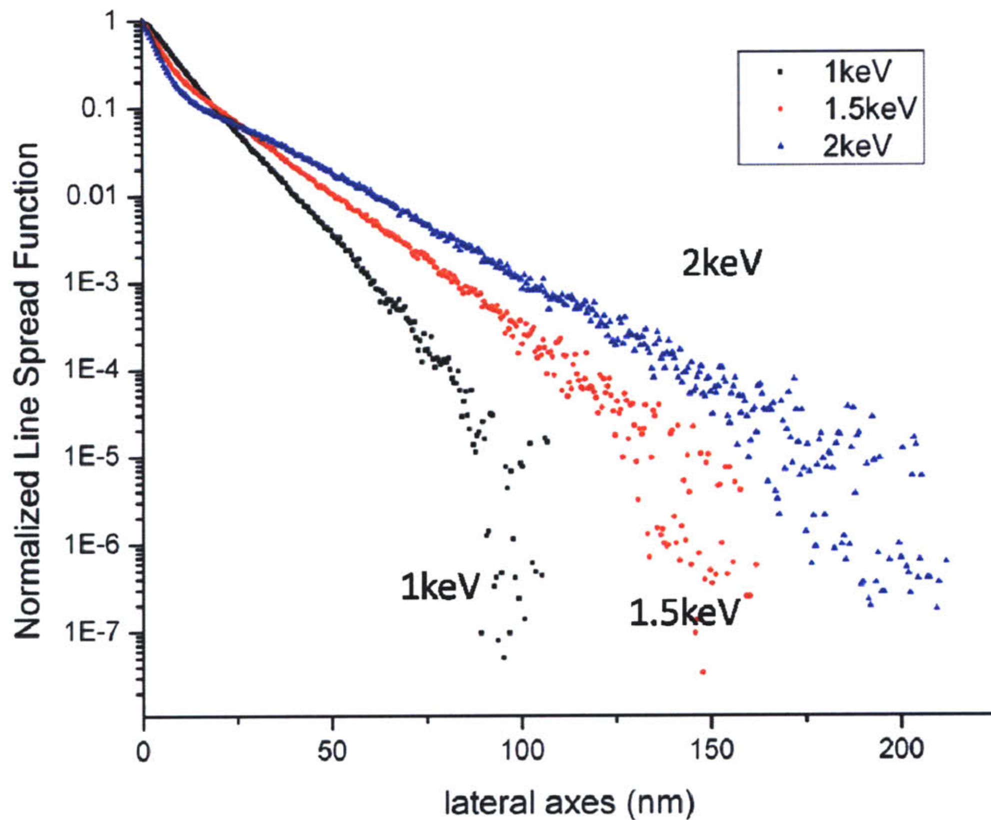

Figure 18. Normalized line spread function with incident energies of 1keV, 1.5keV and 2keV on a layer of 14nm thick HSQ on top of silicon. The 2kV LSF has the smallest full width half maximum, and the 1kV LSF has the widest. Note that proximity effects at distances far away from the center of the cross-section are more evident at higher electron energies. This is consistent with the PSF simulations and experimental results.

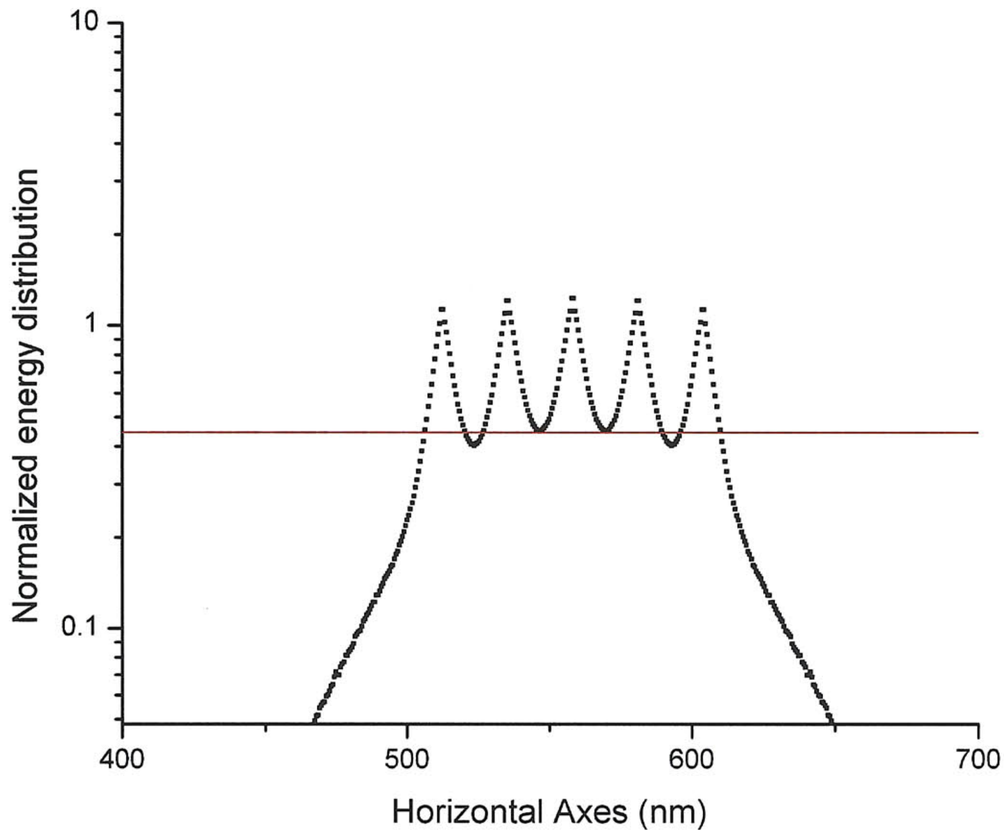

Figure 19. Normalized energy profile of five lines exposed at 2keV in 14nm HSQ on silicon. This plot was obtained by convolving the simulated line-spread function with 5 discrete impulses at 20nm intervals. The red horizontal line is the minimum amount of energy required for HSQ to convert to silicon dioxide. This line is just on or slightly above the energy deposited between the lines, which is consistent with experimental results.

2.4 Pattern Transfer with HSQ as Etch Mask

This section focuses on using reactive-ion etching (RIE) to transfer patterns in HSQ into an underlying anti-reflection coating (ARC) layer. As described in the first chapter, and depicted in Figure 1, the fabrication process does not end when the desired patterns have been successfully developed in the resist. The subsequent challenge is to transfer this pattern into the actual desired material via etching.

A reactive-ion etching system consists of a chamber with two electrodes, as depicted in Figure 20. The etching is carried out under low pressure, with the chamber filled with the etching gas. A radio-frequency (RF) power is applied to the electrode where the substrate is mounted. This RF power generates a plasma that contains ions and chemically reactive species in the form of atoms and radicals. These species can chemically react with the substrate surface to form volatile products. The volatility of these byproducts enables them to quickly desorb from the surface and be removed from the chamber by the vacuum pumping system. Apart from the etching gas, an inert gas such as argon or helium is sometimes added to the gas flow. Positive ions formed from the etching gas and the inert gas bombard the substrate surface, enhancing the vertical etch rate. Hence, an increased directionality and anisotropy can be achieved with ion bombardment [22].

A layer of XHRiC i-line anti-reflection coating polymer (Brewer Science) is first spun on a UV-Ozone-pre-cleaned silicon wafer at 5krpm. The coating was measured by spectroscopic ellipsometer to be 100nm thick. After a post-bake at 150°C for 90s, HSQ was spun on at 5krpm resulting in an approximately 14nm thick layer. Scanning-electron-beam lithography at 2kV was used to expose a pattern of long lines, as shown in Figure 21, into HSQ. HSQ was subsequently developed using salty developer for one minute at room temperature. The sample was then rinsed with DI water to stop the development, and blown dry with nitrogen.

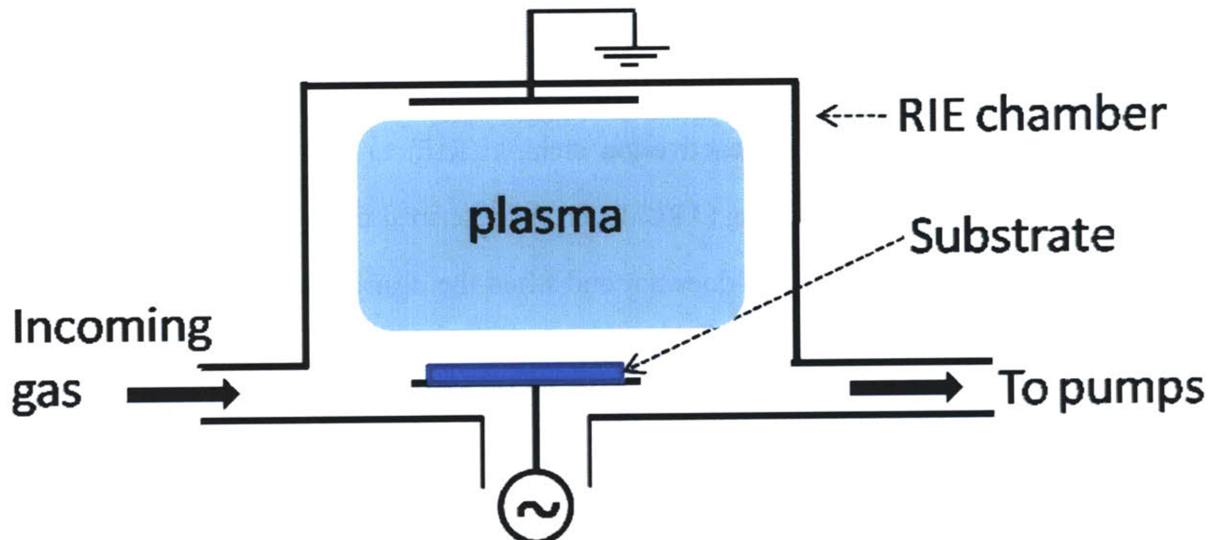

Figure 20. Schematic of a reactive-ion etching chamber. The substrate is placed on the electrode connected to the RF signal while the other electrode (RIE chamber) is grounded. The chamber operates under low pressure and is filled with etching and inert gases. A RF power applied across the electrodes generates a plasma, which contains chemically reactive species. These reactive species react with the substrate surface to produce gases that are removed from the chamber by the vacuum pumping system.

This HSQ line pattern served as an etch mask for the reactive-ion etching process. The polymer XHRiC layer was patterned using RIE in gases oxygen and helium for 50s. A RF power of 145W was applied to generate the plasma, with the dominant etching species being oxygen atoms. These atoms react with the XHRiC layer to produce volatile products such as carbon monoxide and carbon dioxide, which were then removed from the chamber.

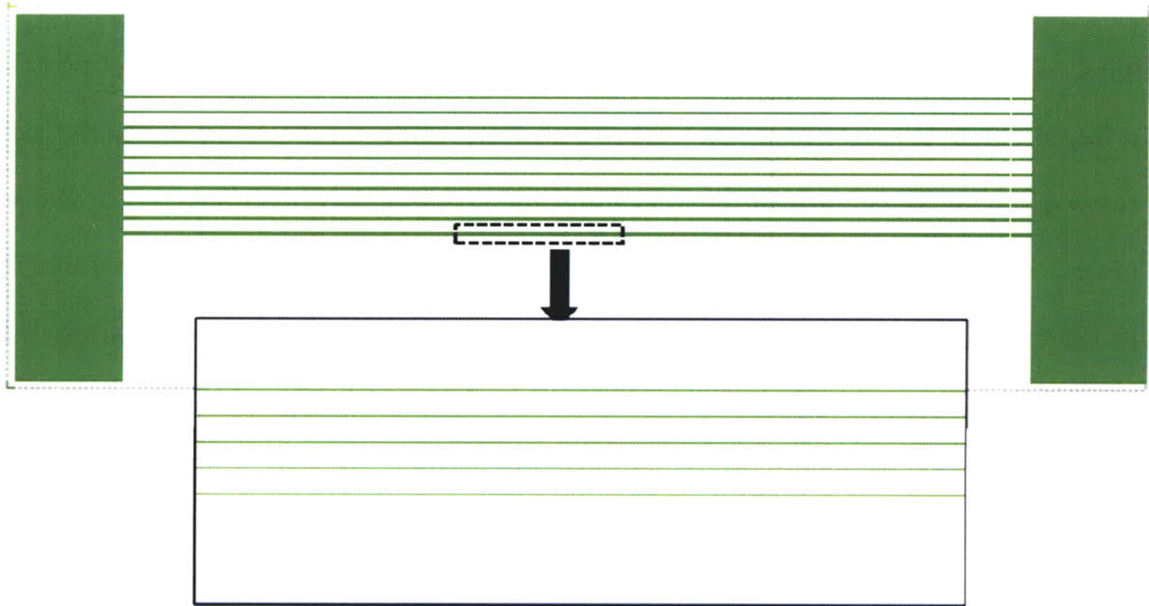

Figure 21. Sketch of pattern used to expose the resist and to demonstrate pattern transfer. The pattern was first written at energy of 2keV into HSQ and developed via salty developer. Next, the pattern acts as etch mask for RIE etching. Long lines (>100μm) were used to facilitate cleaving and cross-section imaging.

Figure 22. Scanning-electron micrograph (top down view) of 40nm pitch lines patterned into 100nm ARC using 14nm HSQ as mask, etched at 145W for 50s. Note that all etched lines are straight.

A top down view of a set of etched XHRiC lines is shown in Figure 22. Note that all etched lines are straight. Special attention has to be paid not to over-etch the lines to prevent structural collapse. After characterizing the etched substrate using top-down imaging, the sample was cleaved across the center of the pattern and the cross-section investigated. The finest pitch of nested lines that could be transferred from a HSQ mask into XHRiC layer was 30nm. Figure 23 shows etched XHRiC lines with pitches of 30nm and 40nm. The lines, measured in the Raith 150, are roughly 9nm thick while the ARC is 60nm high. In the figure, slight bending of the lines is observed. This probably originated from the cleaving process as it was not seen prior to cleaving when imaged top-down.

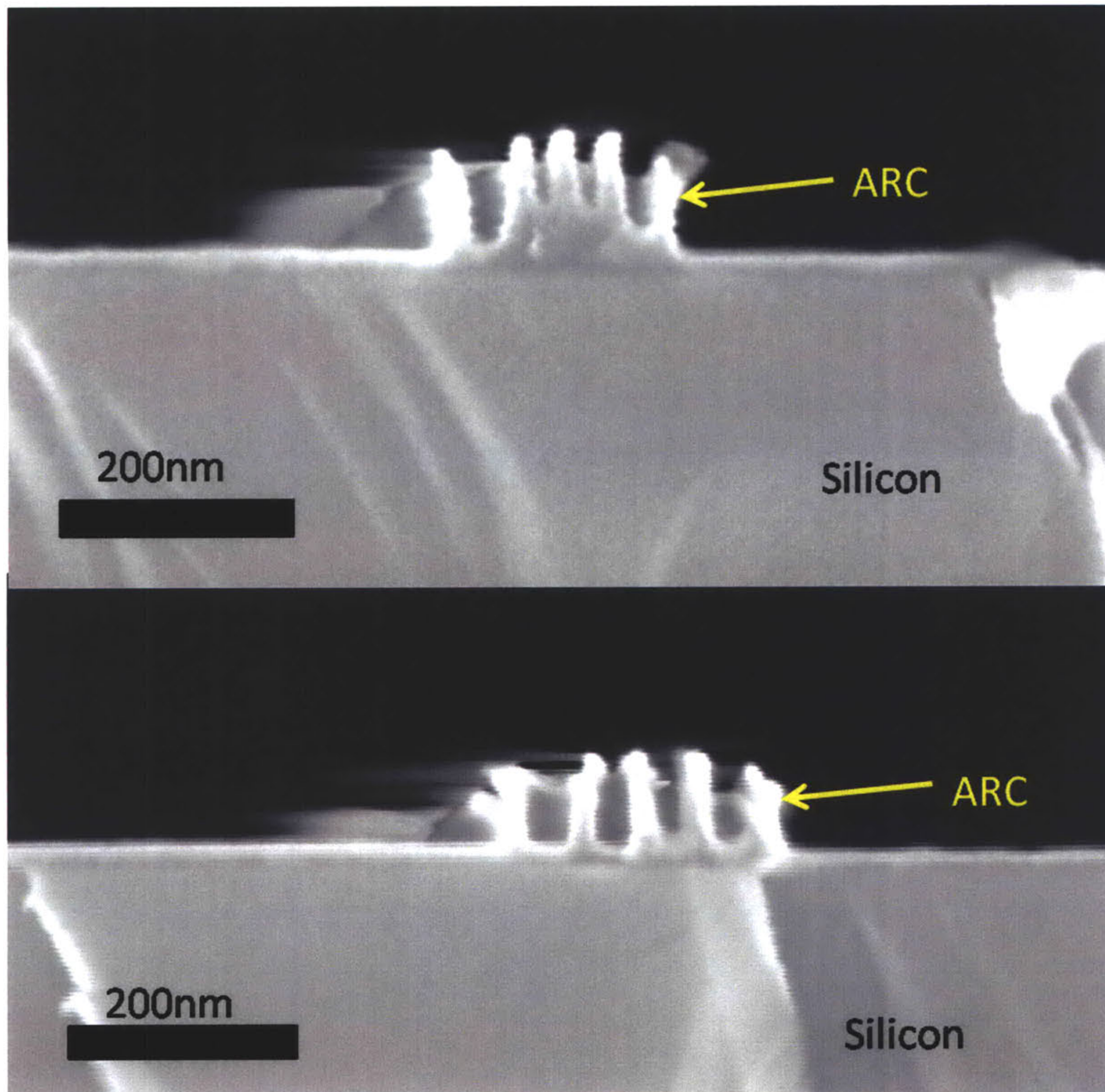

Figure 23. Scanning-electron micrographs of XHRiC cross-sections after reactive-ion-etching for 50s. Electron-beam lithography at energy of 2keV was used to pattern HSQ with lines, which was used as a mask to transfer the pattern into XHRiC. Top micrograph shows the successful pattern transfer with lines at a 30nm pitch, and the bottom micrograph is a cross-section of lines at 40nm pitch. The lines are roughly 9nm wide and the XHRiC approximately 60nm thick. Slight bending of the lines observable in both micrographs probably originated from the cleaving process or charging.

Chapter 3

SPLEBL Reference Grid Fabrication and Signal Contrast Measurements

The reference grid is an essential component of SPLEBL, providing a feedback signal for the electron-beam position correction. The *fabrication* process of SPLEBL reference grid for low voltages has to satisfy multiple requirements. First, the reference grid fabrication process should not expose or affect the electron-beam resist. Second, the periodic reference grid must have long-range spatial-phase coherence (i.e. free from distortion). Lastly, the fabrication steps should be relatively simple.

Previously, a PDMS stamp was used to print grids of aminopropyl-triethoxy-silane (APTES) [23]. Although this method is quick and simple, stamping introduces distortions in the reference grid. Interference lithography has been shown to produce periodic grids and gratings with long-range coherence-phase coherence in a reliable manner. This chapter investigates the possibility of fabricating a photoresist reference grid for low-voltage SPLEBL with interference lithography, and also compares the secondary-electron signal of this photoresist grid with respect to a reference sample. A schematic of the proposed photoresist grid on top of electron-beam resist with a thin conducting aluminum interlayer is depicted in Figure 24.

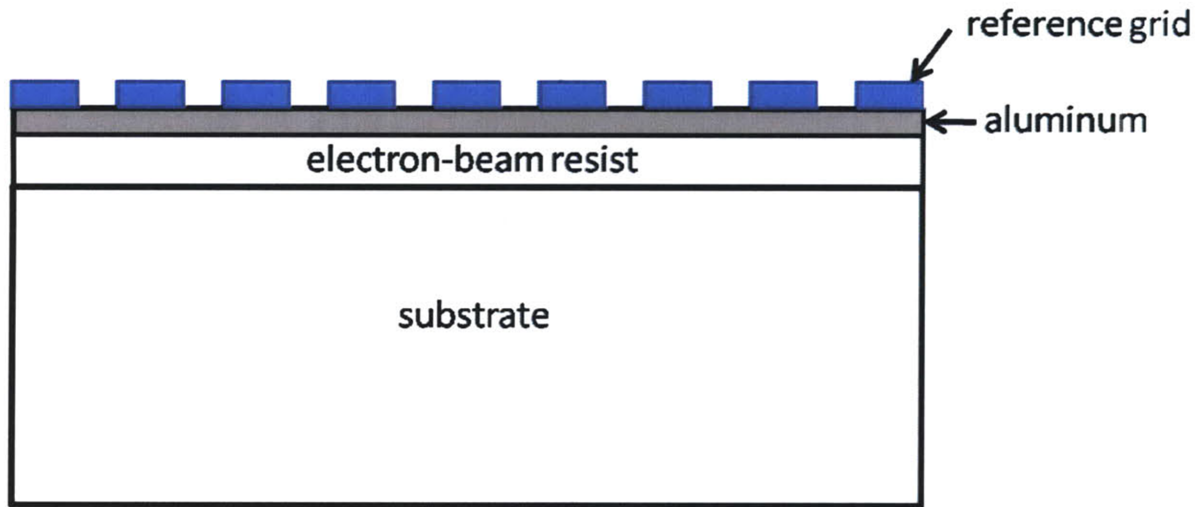

Figure 24. Schematic of the proposed photoresist grid on top of electron-beam resist with a thin, conducting aluminum interlayer. The reference grid is fabricated using interference lithography, which provides the reference grid with long-range spatial-phase coherence. A thin aluminum interlayer is used to prevent charging during the exposure process.

There is also an additional requirement on the reference grid: it must have a minimal impact on the resolution of low-voltage scanning-electron-beam lithography. Due to the short penetration depth of low-energy electrons, this implies that the reference grid and the aluminum interlayer must be thin enough to avoid significant electron scattering.

The accuracy of the feedback loop depends heavily on the strength of the feedback signal relative to the noise in the signal; the important metric is the signal-to-noise ratio (SNR). This SNR depends on multiple factors: secondary-electron yield of the material, dwell time or scanning speed of the beam, and noise in the secondary-electron detectors. Apart from secondary-electron yield, the other factors are dependent on the exposure conditions and lithography system itself. These will not be explored further.

The secondary-electron yield (SEY) is defined as the number of secondary electrons emitted per incident electron. Secondary-electron yield depends on the material and its thickness. Generally, a higher atomic number (Z) material provides a higher secondary-electron yield, while a thicker reference grid increases the possibility of electron interaction and hence increased signal, until the thickness exceeds the secondary electron diffusion length. Figure 25 is a compilation of secondary electron yield values in the literature with an incoming electron energy of 30keV. Note that even for the same material there is a significant variation in the measured secondary-electron yield and it is unclear what value to choose. This variation probably originates from sample processing (e.g. thickness of oxide layer or contamination), how the secondary-electron yield was measured, and chamber conditions. Thus for the purpose of investigating the strength of the secondary-electron signal, *signal levels* between the photo-resist grid and a reference sample is used as elaborated further in other sections of this chapter.

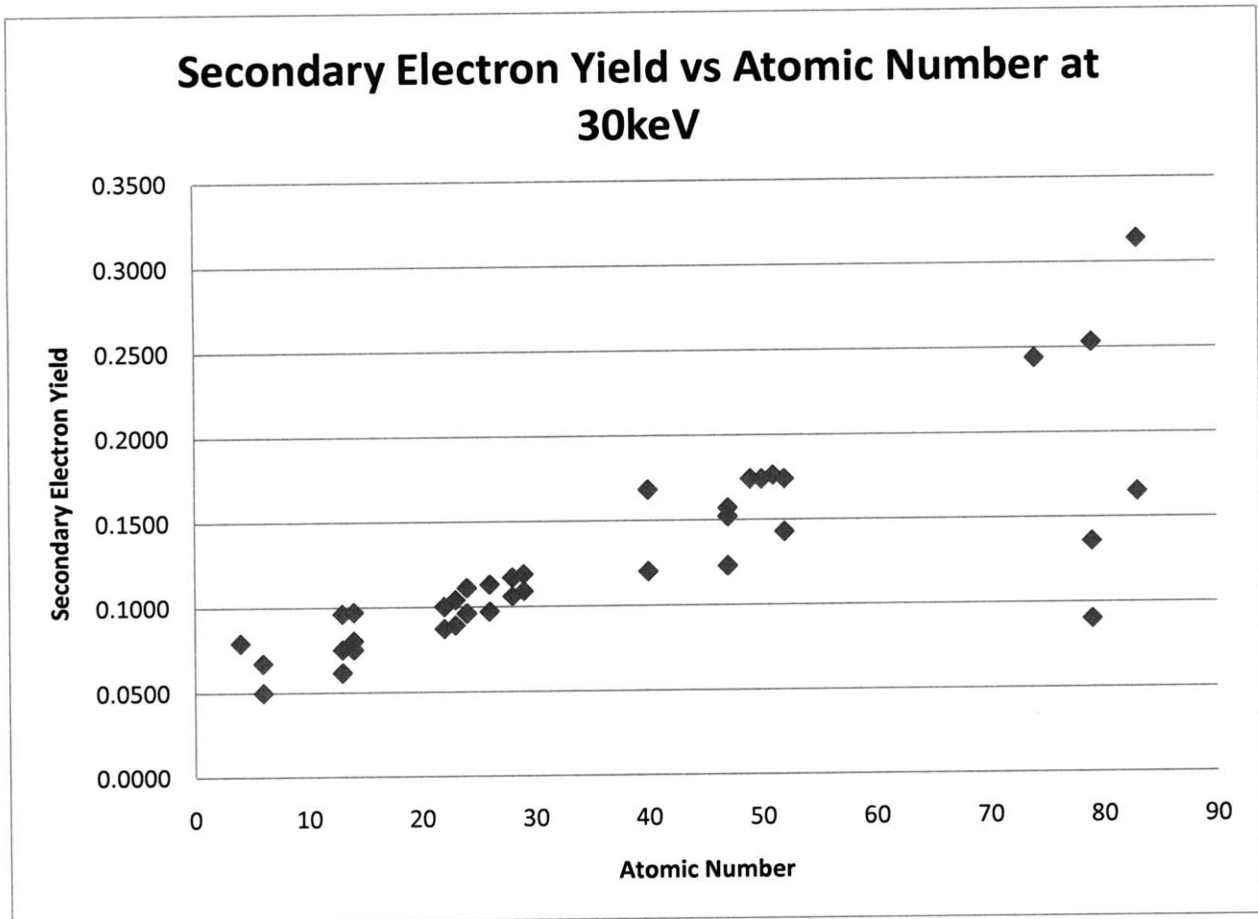

Figure 25. Compilation from literature of experimentally-measured secondary electron yield versus atomic number at an electron energy of 30keV.

3.1 Lloyd's Mirror Interference Lithography

Interference lithography is used to fabricate grids and gratings with long-range spatial-phase coherence. This method generates a standing wave pattern by interfering two coherent beams, with the period of the standing wave determined by the angle between the two beams. A photoresist layer sensitive to the radiation wavelength is exposed to the standing wave pattern, and the irradiated areas undergo chemical changes that change the dissolution rate of the resist. Subsequent immersion of the sample in these solutions selectively removes the photoresist.

Lloyd's Mirror interference lithography was chosen instead of Mach-Zehnder interference lithography due to the relative simplicity (single beam, minimal alignment) of the Lloyd's Mirror setup, which is depicted in Figure 26. A He-Cd laser with 325nm wavelength produces a TEM00 Gaussian beam with 30cm coherence length. This beam is passed through a spatial filter to remove high-frequency noise, and then expanded for roughly 2m to fill the area containing the aluminum holder, substrate, and mirror. A highly-reflective aluminum mirror (flat to $\lambda/4$) placed normal to the substrate reflects the laser light, which interferes with the unreflected incident light to form a standing wave pattern at the substrate. The angle between the light and the setup determines the period of the standing wave pattern. Spatial periods as fine as 180nm can be fabricated using the Lloyd's Mirror setup. The substrate is held in place on the holder by vacuum for mechanical stability. Single exposures produces gratings, while double exposures (with the substrate rotated 90° after first exposure) produces grids in a quick and reliable manner.

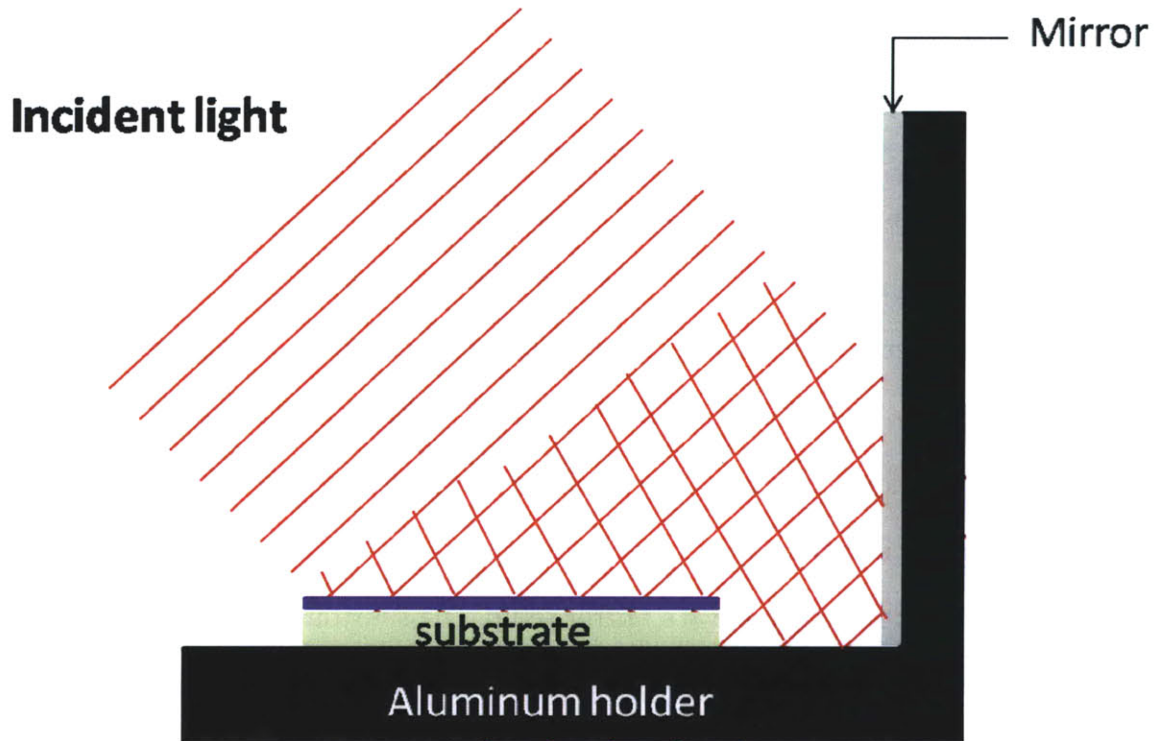

Figure 26. Schematic of a Lloyd's Mirror interference-lithography setup. A highly-reflective aluminum mirror (flat to $\lambda/4$) placed normal to the substrate reflects the laser light. This reflected light interferes with the unreflected incident light to form a standing wave pattern at the substrate, which is coated with a radiation-sensitive resist. The substrate is attached to the aluminum holder by vacuum for mechanical stability. The angle between the laser light and the setup determines the period of the standing wave pattern.

A highly-absorbing anti-reflection coating (ARC) is almost always placed under a photoresist to reduce the amount of light reflected from the substrate back into the photoresist. This eliminates undesired additional standing wave patterns in the resist in the vertical direction (normal to the resist). For SPLEBL, an ARC cannot be used as the photoresist layer needs to be placed directly on top of either a conducting, low-Z interlayer or directly on top of the electron-beam resist. Fortunately, due to the thinness of the resist used in the experiments

(<50nm), relative to the incident wavelength, this standing wave problem can be neglected. However, without an ARC layer, the amount of back-reflected light is very sensitive to thickness and type of material below the photoresist, as well as the photoresist itself. The amount of back-reflected light should be calculated, and the exposure time adjusted accordingly, for any specific resist stack.

Sumika photoresist PFI-88 A2 was used in the experiments in this section. Undiluted PFI-88 achieves a thickness of ~225 nm when spun at 3krpm. This is far thicker than desired. To obtain thinner resists, PFI-88 was diluted with heptanone at ratios ranging up to 1:10. A plot of the resist thickness versus dilution ratio is shown Figure 27. The final resist thickness was determined using atomic-force microscope on grids or gratings exposed by interference lithography, as shown in Figure 28. The minimum resist thickness obtained at dilution ratio1:10 was 11nm thick.

Silicon wafers were first cleaned with UV-Ozone to remove organic residue on the substrate surface, with the cleanliness of the surface verified using the steam nucleation test. This confirmed the presence of a thin oxide, i.e. wetting. The adhesion promoter, hexamethyldisilazane (HMDS) was spin-coated at 2krpm. The presence of HMDS on the silicon wafer was confirmed with the steam nucleation test (i.e. non-wetting). PFI-88 was then spin-coated onto the HMDS-primed wafer at 3krpm, followed by a pre-bake at 90°C for 90s. The resist was then exposed with Lloyd's Mirror interference lithography with incident energies per cm^2 between 10mJ and 30mJ, depending on the film thickness. The sample is then immersed in Shipley's Microposit MF CD-26 developer for 60s, rinsed with DI water and blown dry with nitrogen. A scanning-electron micrograph of a developed grid is shown in Figure 29.

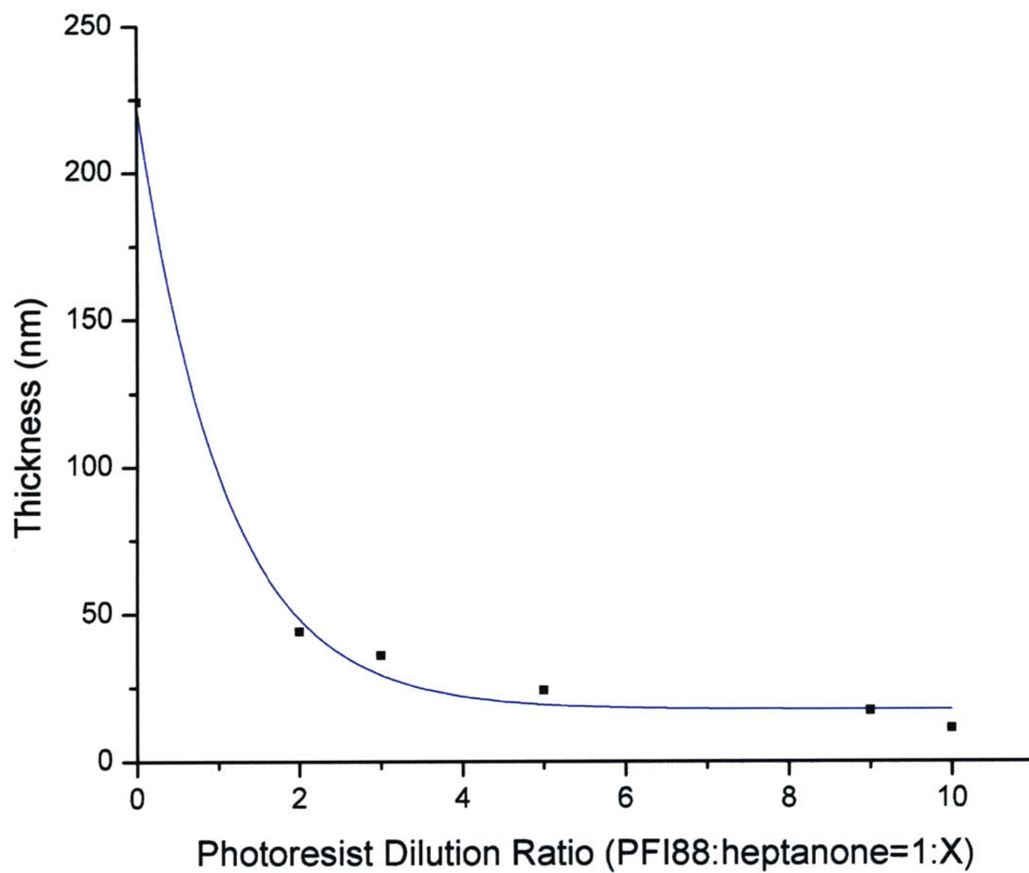

Figure 27. Plot of thickness of photoresist PFI-88 at a range of dilution ratio. The black dots are data points that were experimentally determined using the atomic-force microscope. The blue line is an exponential fit to the data points.

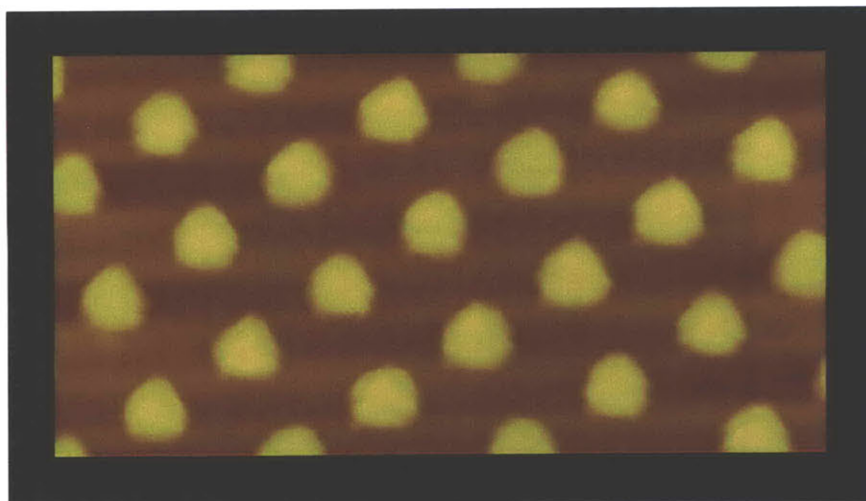

Figure 28. Atomic-force microscope scan of a 44 nm thick PFI-88 grid on silicon. The substrate was first UV-Ozone cleaned for 10 minutes. HMDS was then spun on at 2krpm followed by photoresist PFI-88(PFI-88:heptanone=1:2) at 3kprm. The sample was then baked at 90 °C for 90s and exposed to 325nm light using Lloyd's Mirror interference lithography. Subsequently, the sample was developed in CD-26 for 60s, cleaned with DI water and blown dry with nitrogen. The period of the grid is 600nm.

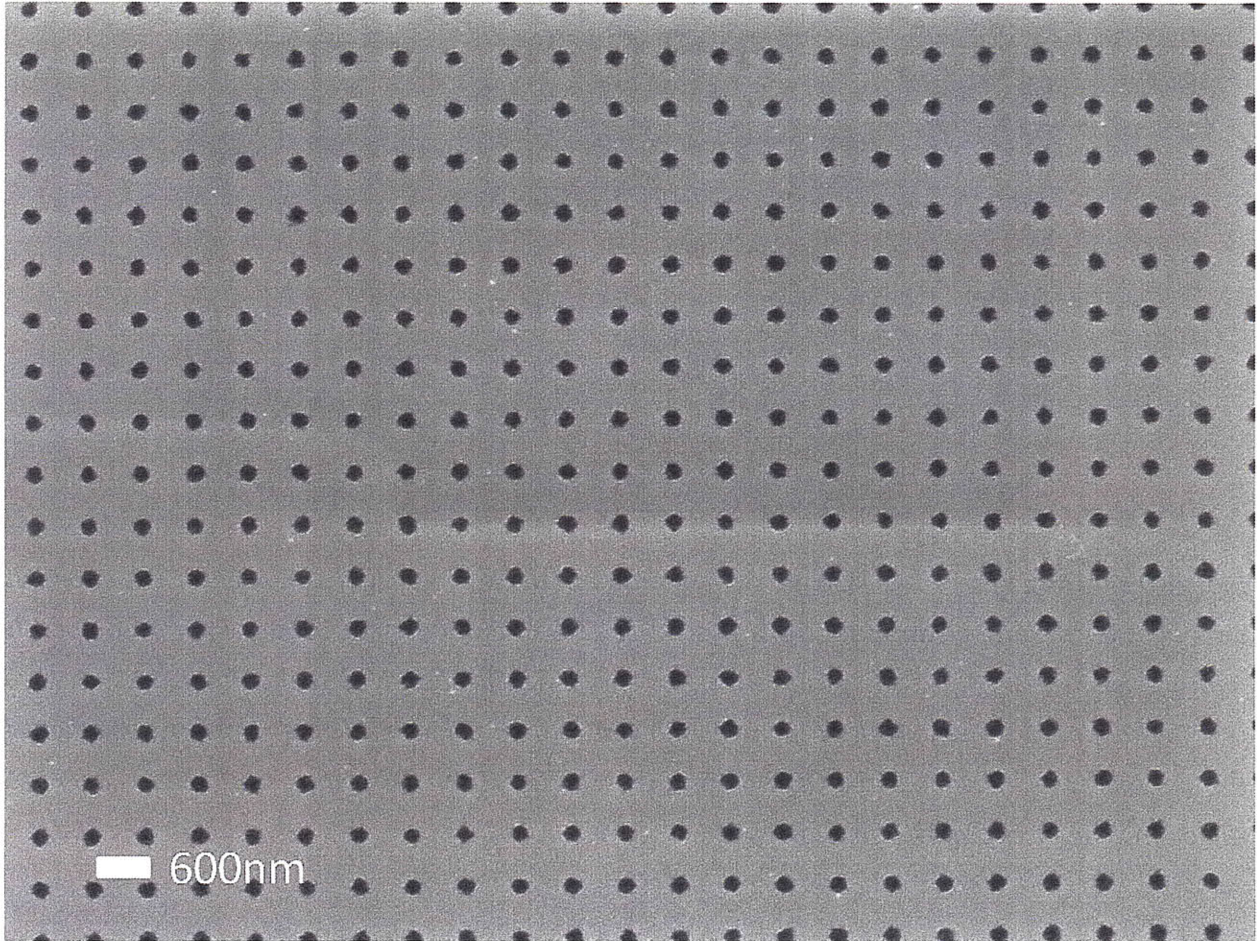

Figure 29. Scanning-electron micrograph of photo-resist PFI-88 imaged at an electron energy of 2keV. The dark spots are the photoresist, and the lighter areas are silicon. The period of the grid is 600nm.

3.2 Signal-Contrast Measurements with sub-2keV Electrons

The secondary electron yield (SEY) is defined as the number of secondary electrons emitted for an incoming electron. It was depicted in Figure 25 that the SEY increases with increasing atomic number (Z). For a given material, the SEY also varies as the incident beam energy changes. Most materials exhibit a peak, usually at voltages less than 500eV, as depicted in Figure 30.

Unfortunately, it is very difficult to accurately measure the secondary-electron yield of a particular material as it is influenced by many parameters. The crystallinity of the material, the method which the material was deposited, the surface conditions of the material, vacuum conditions and measurement conditions affect the SEY of a material.

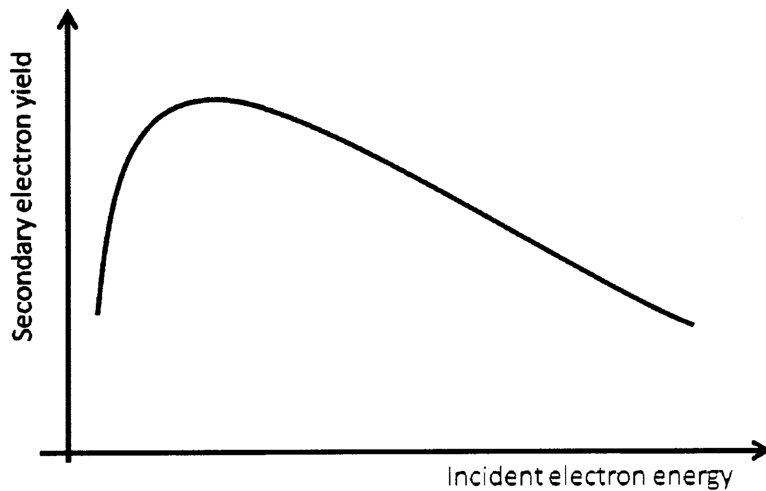

Figure 30. The characteristic secondary-electron yield (SEY) curve for many materials. The SEY initially increases as the energy increases, but then decreases with further increase in incident electron energy. The peak generally occurs at incident electron energy of less than500eV.

A partial goal of this thesis is to investigate the possibility of using photoresist to provide a secondary-electron signal for SPELBL. Currently, the only material that has been investigated for low-voltage SPLEBL is aminopropyl-triethoxy-silane (APTES), a silane-based self-assembled monolayer. Thus, it is sufficient to compare the relative strength of the signal from photoresists to signal obtained from aminopropyl-triethoxy-silane (APTES).

Signal-level relative to a reference sample is the important metric. Since the photoresist was spin-coated on a silicon wafer, it is logical to use similar silicon wafers as the reference

sample. Photoresists at different thicknesses was imaged at 1kV, 1.5kV and 2kV in the presence of a Faraday Cup and the reference sample, as shown in Figure 31. The Faraday Cup signal establishes the zero level. This value is then subtracted from the signal of the photoresist-on-silicon sample and the reference sample. The reference-sample signal is then scaled to a fixed value and signal from the photoresist-on-silicon sample scaled accordingly. This ensures accurate comparisons from sample to sample. This approach is also used to measure the signal level from aminopropyl-triethoxy-silane (APTES). All measurements were conducted using the Raith 150.

A plot of the signal level for photoresists of various thicknesses as a function of incident electron energy is shown in Figure 32. The signal level of APTES with respect to a reference sample is also shown. A signal level of one corresponds to the signal from the reference silicon sample. The photoresist samples and the APTES samples all show similar trends, with the signal level increasing with increasing incident electron energy. The APTES signal level is much higher than the signal from photoresist samples. Interestingly, the signal level from a 17nm-thick photoresist is lower than that from a 11nm-thick and a 24nm-thick photoresist samples. A plot as a function of photoresist thickness is in Figure 33. The signal level is not linear with increasing photoresist thickness for all incident electron energies measured. Currently, it is unclear why the signal contrast varies in such a manner.

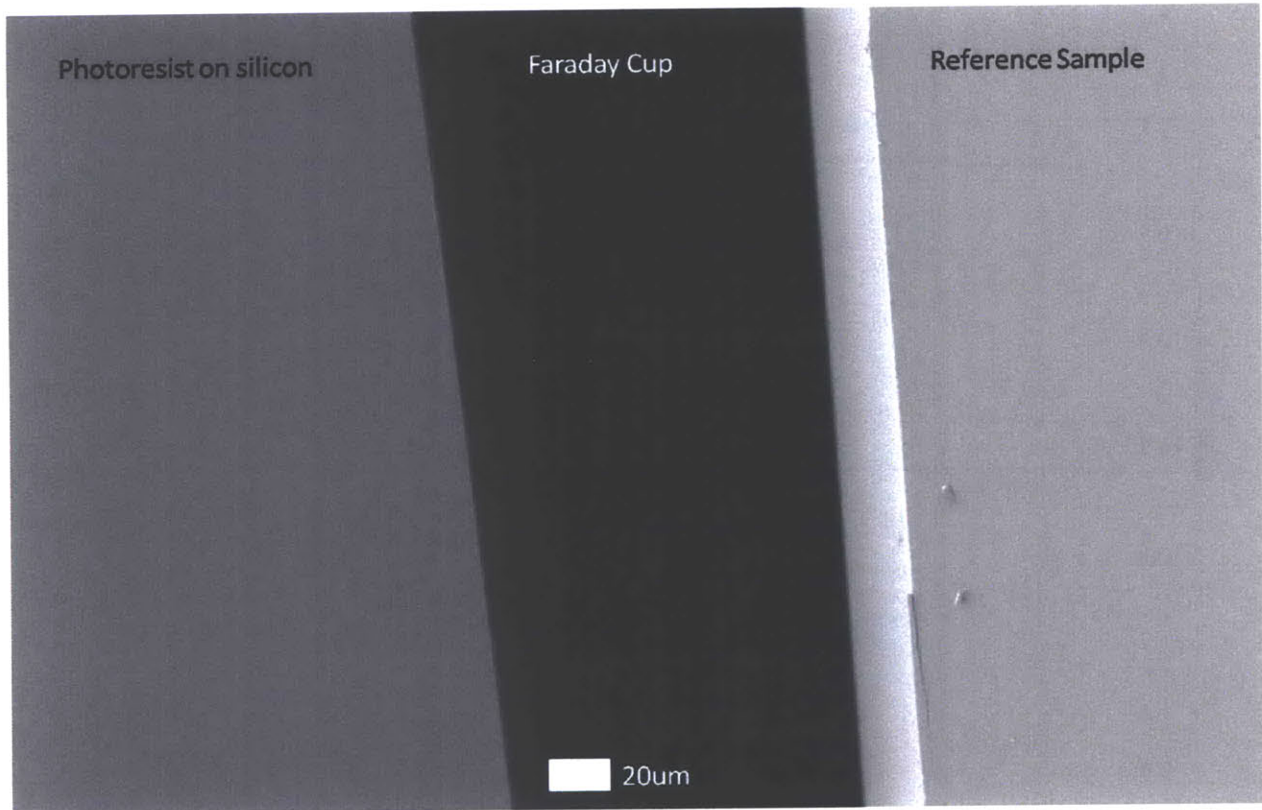

Figure 31. Scanning-electron micrograph of a photoresist-on-silicon, Faraday-Cup and the reference sample. The Faraday Cup provides the zero signal level, which is then subtracted from the signal strength of the photoresist and reference sample. The signal level of the reference sample is then scaled to a fixed value, and the signal from the photoresist-on-silicon is scaled similarly. This ensures accurate measurements from sample to sample. The reference sample is UV-Ozone cleaned just before imaging to ensure surface cleanliness.

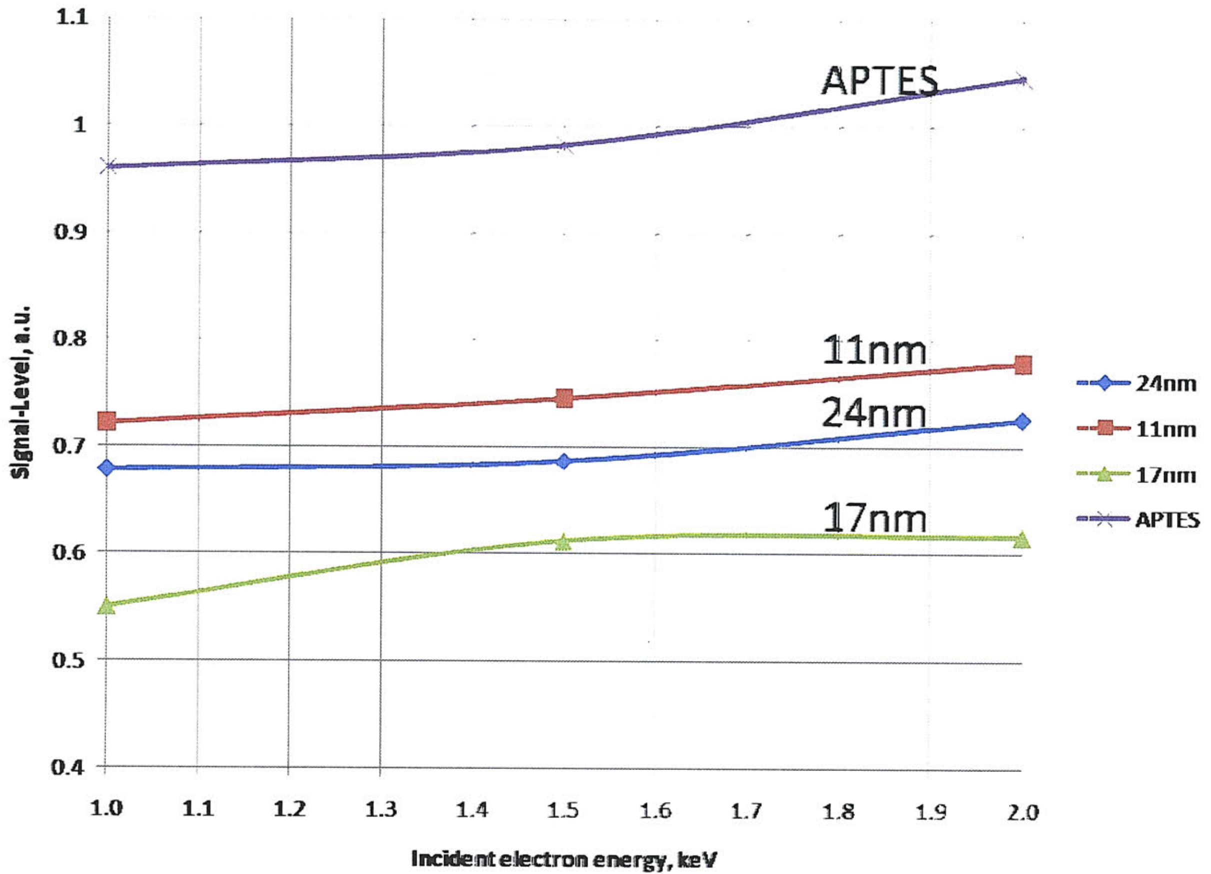

Figure 32. Plot of signal level vs incident electron energy for photoresist at various thickness and also amino-propyl-triethoxysilane (APTES), with silicon as reference sample. All samples show a similar trend, where the signal contrast increases with increasing incident electron energy. A signal contrast of one corresponds to the signal level of the reference silicon sample.

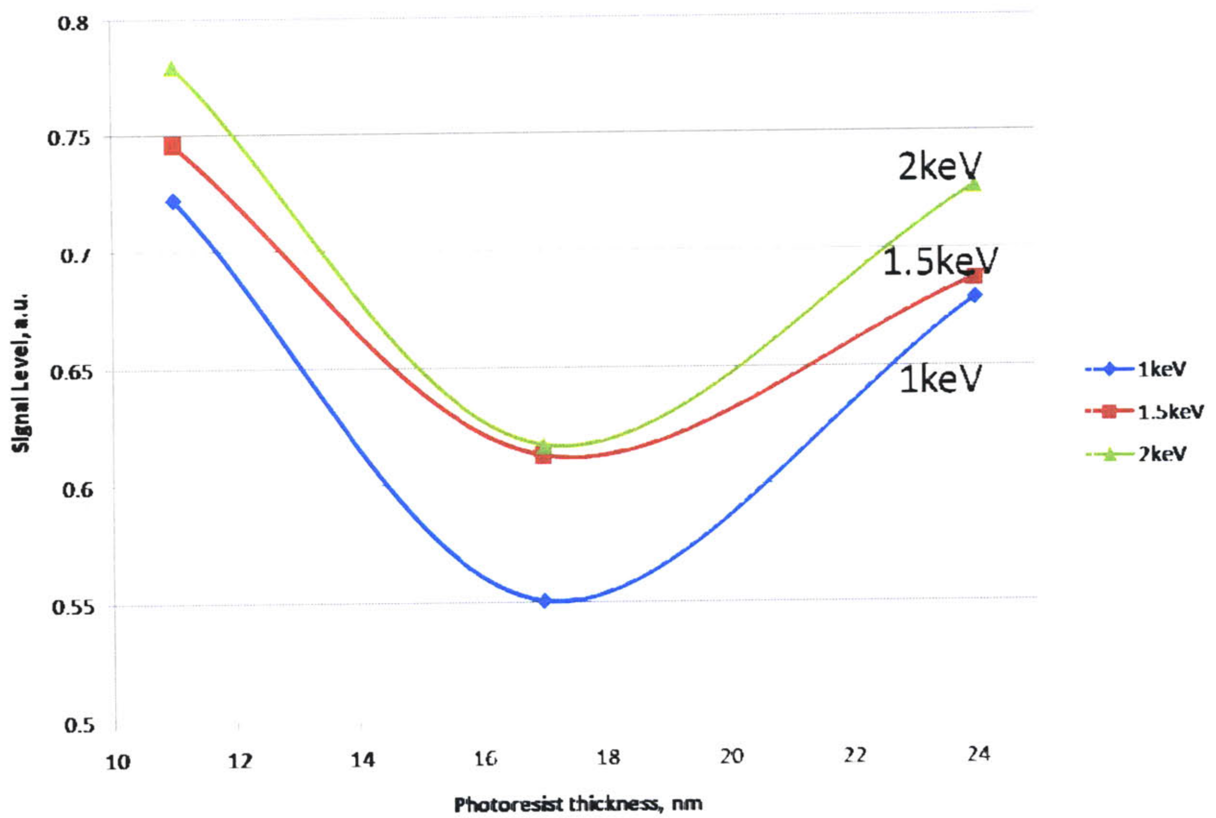

Figure 33. Plot of signal level vs photoresist thickness. Note the dip in signal contrast as the photoresist thickness increases.

Chapter 4

Conclusion

The research in this thesis has confirmed that good resolution for dense patterns is achievable with low-voltage scanning-electron-beam lithography. Nested L's with pitches as fine as 20nm can be patterned in HSQ at incident electron energy of 2keV and 1.5keV, while the smallest pitch achieved at 1keV is 25nm. Monte-Carlo simulations of energy distributions in a resist caused by low-voltage electrons agree with the experimental results.

The signal contrast of photoresist at varying thickness with respect to a reference silicon sample was measured. Signal contrast of APTES, the only material previously used for low-voltage SPLEBL, was also measured. The signal contrast of APTES is higher than the signal contrast from photoresist at all voltages and thickness measured.

References

[1] A.E. Grigorescu and C.W. Hagen, "Resists for sub-20-nm electron beam lithography with a focus on HSQ: state of the art.," *Nanotechnology*, vol. 20, 2009, p. 292001.

[2] J. Ferrera, "Nanometer-Scale Placement in Electron-Beam Lithography," 1999.

[3] *Microlithography: Science and Technology*, Marcel Dekker, Inc., 1998.

[4] M.J. Madou, *Fundamentals of Microfabrication: The Science of Miniaturization*, CRC Press, 2002.

[5] A. Murray, M. Scheinfein, and M. Isaacson, "Radiolysis and resolution limits of inorganic halide resists," *Journal of Vacuum Science & Technology B: Microelectronics and Nanometer Structures*, vol. 3, 1985, p. 367.

[6] L.D. Jackel, R.E. Howard, P.M. Mankeiwich, H.G. Craighead, and R.W. Epworth, "Beam energy effects in electron beam lithography: The range and intensity of backscattered exposure," *Applied Physics Letters*, vol. 45, 1984, p. 698.

[7] P.A. Peterson, Z.J. Radzimski, S.A. Schwalm, and P.E. Russell, "Low-voltage electron beam lithography," *Journal of Vacuum Science & Technology B: Microelectronics and Nanometer Structures*, vol. 10, 1992, p. 3088.

[8] F. Zhang, H.I. Smith, and J. Dai, "Fabrication of high-secondary-electron-yield grids for spatial-phase-locked electron-beam lithography," *Journal of Vacuum Science & Technology B: Microelectronics and Nanometer Structures*, vol. 23, 2005, p. 3061.

[9] J.T. Hastings, F. Zhang, and H.I. Smith, "Nanometer-level stitching in raster-scanning electron-beam lithography using spatial-phase locking," *Journal of Vacuum Science & Technology B: Microelectronics and Nanometer Structures*, vol. 21, 2003, p. 2650.

[10] a. Olkhovets and H.G. Craighead, "Low voltage electron beam lithography in PMMA," *Journal of Vacuum Science & Technology B: Microelectronics and Nanometer Structures*, vol. 17, 1999, p. 1366.

[11] A. Tilke, M. Vogel, F. Simmel, A. Kriele, R.H. Blick, H. Lorenz, D.A. Wharam, J.P. Kotthaus, and I. Introduction, "Low-energy electron-beam lithography using calixarene," *Applied optics*, vol. 25, 1986, p. 4228.

[12] D.M. Tanenbaum, "High resolution electron beam lithography using ZEP-520 and KRS resists at low voltage," *Journal of Vacuum Science & Technology B: Microelectronics and Nanometer Structures*, vol. 14, 1996, p. 3829.

[13] S.R. Wasserman, G.M. Whitesides, I.M. Tidswell, B.M. Ocko, P.S. Pershan, and J.D. Axe, "The structure of self-assembled monolayers of alkylsiloxanes on silicon: a comparison of results from ellipsometry and low-angle x-ray reflectivity," *Journal of the American Chemical Society*, vol. 111, 1989, pp. 5852-5861.

[14] J.A. Woollam, *A Short Course in Ellipsometry*.

[15] K.E. Gonsalves, L. Merhari, H. Wu, and Y. Hu, "Organic–Inorganic Nanocomposites: Unique Resists for Nanolithography," *Advanced Materials*, vol. 13, 2001, pp. 703-714.

[16] A. Jamieson, C.G. Willson, Y. Hsu, and A.D. Brodie, "Low-voltage electron beam lithography resist processes: top surface imaging and hydrogen silisesquioxane bilayer," *Journal of Microlithography, Microfabrication, and Microsystems*, vol. 3, 2004, p. 442.

[17] I. Haller, M. Hatzakis, and R. Srinivasan, "High-resolution Positive Resists for Electron-beam Exposure," 1968, pp. 251-256.

[18] H. Namatsu, "Three-dimensional siloxane resist for the formation of nanopatterns with minimum linewidth fluctuations," *Journal of Vacuum Science & Technology B: Microelectronics and Nanometer Structures*, vol. 16, 1998, p. 69.

[19] J.K. Yang and K.K. Berggren, "Using high-contrast salty development of hydrogen silsesquioxane for sub-10-nm half-pitch lithography," *Electrical Engineering*, 2007, pp. 2025-2029.

[20] V. Manfrinato, "Private Communication."

[21] S. Luo, X. Zhang, and D.C. Joy, "Joy Electron stopping power.pdf," *Radiation Effects and Defects in Solids*, vol. 117, 1991, pp. 235-242.

[22] J. Coburn, *Plasma Etching and Reactive Ion Etching*, American Institute of Physics, 1982.

[23] C.B. Samantaray and J.T. Hastings, "Amino-propyl-triethoxy-silane on aluminum fiducial grids for spatial-phase-locked electron-beam lithography," *Journal of Vacuum Science & Technology B: Microelectronics and Nanometer Structures*, vol. 27, 2009, p. 2558.